bioRxiv preprint doi: https://doi.org/10.1101/818047; this version posted October 24, 2019. The copyright holder for this preprint (which was not certified by peer review) is the author/funder, who has granted bioRxiv a license to display the preprint in perpetuity. It is made available under aCC-BY 4.0 International license.

Sensitivity and uncertainty analysis of two human atrial cardiac cell models using Gaussian process emulators

Sam Coveney[1], Richard H. Clayton[1*].

Insigneo Institute for *in-silico* Medicine and Department of Computer Science, University of Sheffield, Sheffield, UK.

* r.h.clayton@sheffield.ac.uk

Abstract

Cardiac cell models reconstruct the action potential and calcium dynamics of cardiac myocytes, and are becoming widely used research tools. These models are highly detailed, with many parameters in the equations that describe current flow through ion channels, pumps, and exchangers in the cell membrane, and so it is difficult to link changes in model inputs to model behaviours. The aim of the present study was to undertake sensitivity and uncertainty analysis of two models of the human atrial action potential. We used Gaussian processes to emulate the way that 11 features of the action potential and calcium transient produced by each model depended on a set of. The emulators were trained by maximising likelihood conditional on a set of design data, obtained from 300 model evaluations. For each model evaluation, the set of inputs was obtained from uniform distributions centred on the default values for each parameter, using latin-hypercube sampling. First order and total effect sensitivity indices were calculated for each combination of input and output. First order indices were well correlated with the square root of sensitivity indices obtained by partial least squares regression of the design data. The sensitivity indices highlighted a difference in the balance of inward and outward currents during the plateau phase of the action potential in each model, with the consequence that changes to one parameter can have opposite effects in the two models. Overall the interactions among inputs were not as important as the first order effects, indicating that model parameters tend to have independent effects on the model outputs. This study has shown that Gaussian process emulators are an effective tool for sensitivity and uncertainty analysis of cardiac cell models.

Author summary

The time course of the cardiac action potential is determined by the balance of inward and outward currents across the cell membrane, and these in turn depend on dynamic behaviour of ion channels, pumps and exchangers in the cell membrane. Cardiac cell models reconstruct the action potential by representing transmembrane current as a set of stiff and nonlinear ordinary differential equations. These models capture biophysical detail, but are complex and have large numbers of parameters, so cause and effect relationships are difficult to identify. In recent years there has been an increasing interest in uncertainty and variability in computational models, and a number of tools have been developed. In this study we have used one of these tools, Gaussian process emulators, to compare and contrast two models of the human atrial action potential. We obtained sensitivity indices based on the proportion of variance in a model output

bioRxiv preprint doi: https://doi.org/10.1101/818047; this version posted October 24, 2019. The copyright holder for this preprint (which was not certified by peer review) is the author/funder, who has granted bioRxiv a license to display the preprint in perpetuity. It is made available under aCC-BY 4.0 International license.

that is accounted for by variance in each of the model parameters. These sensitivity indices highlighted the model parameters that had the most influence on the model outputs, and provided a means to make a quantitative comparison between the models.

Introduction

The cardiac action potential arises from the movement of ions through channels, pumps, and exchangers in the cell membrane. At any instant, the current carried by each ionic species depends on potential difference across the cell membrane, as well as ion concentrations and the dynamics of ion channel gating. The complex interplay of currents produces depolarisation and then repolarisation of the membrane, which then acts to trigger release of Ca^{2+}, initiating mechanical contraction.

The first model of the action potential in a cardiac myocyte was developed over 50 years ago [1], and since then a series of more detailed models have been developed as experimental techniques and data have improved. The present generation of models provide detailed reconstructions of the cardiac action potential [2], and computational models of cardiac cells and tissue have become valuable research tools because they can encode biophysical mechanisms into a quantitative framework, and so can be used to test and construct hypotheses [3].

Although these detailed models are capable of simulating the behaviour of real cardiac myocytes, this veracity comes at the price of complexity. Models of the cardiac action potential typically comprise a system of coupled, stiff, and non-linear ordinary differential equations. There are many model parameters and boundary conditions, which we will refer to as *model inputs* from here onward. These model inputs can be derived from experimental data, using approaches based on those pioneered by Hodgkin and Huxley in squid giant axon [4]. However, experimental data are subject to variability and error arising from both limitations of experimental methods as well as intrinsic variability in cardiac cells. Some of these inputs, such as binding affinities and reaction rate constants, can be considered to have fixed values because they have a physical basis. However others, such as maximum ion channel conductance, depend on the ion channel density in the cell membrane as well as other factors that are variable. These quantities may therefore vary from one cell to another, and even from beat to beat in the same cell. These considerations underlie three specific problems. First, errors and variability in data are typically not taken into account when fitting model inputs, and taking an average of experimental data can distort model behaviour [5]. Second, data from different sets of experiments can result in different models of the same cell type. For example, there are several models of the human atrial action potential, all based on human data, but which show different types of behaviour [6, 7]. Finally, a further complication arises from the modular nature of cardiac cell models. The equations for a particular ion channel, pump, or exchanger are often re-used in different models and so the provenance of model inputs may be very difficult to establish [8].

Addressing these problems requires approaches that can establish how model behaviours and outputs depend on inputs that may be uncertain. However, the level of detail included in the present generation of cardiac cell models means that formal analysis is difficult, and so a detailed examination of how model inputs influence outputs relies on large numbers of numerical simulations where the inputs vary from one model run to the next [9]. These datasets can be used for regression analysis, which enables the sensitivity of model outputs to changes in model inputs to be assessed [10]. Another approach is to select a set of inputs, or population of models, that produce action potentials that are in the range of experimental observations [11–13]. A drawback of these approaches arises from the high dimensional input space for the models; a very large number of model evaluations is needed to investigate the input

bioRxiv preprint doi: https://doi.org/10.1101/818047; this version posted October 24, 2019. The copyright holder for this preprint (which was not certified by peer review) is the author/funder, who has granted bioRxiv a license to display the preprint in perpetuity. It is made available under aCC-BY 4.0 International license.

space thoroughly [14], although recent work indicates that this challenge can be overcome by new models that are designed for uncertainty quantification [15].

Methods to quantify uncertainty and variability using probabilistic approaches have been developed and applied in a number of areas [16], including cardiovascular flow models [17]. These approaches are promising because an emulator of a computational model can treat uncertainties explicitly, and can be evaluated at much lower computational cost than the original model [19, 42]. Gaussian Processes are flexible non-parametric regression tools capable of fitting complex data, thus they are widely used in the machine learning community. They provide confidence intervals on their predictions, and are therefore ideal tools for sensitivity and uncertainty analysis.

In this report we demonstrate the use of Gaussian process emulators for sensitivity and uncertainty analysis of two biophysically detailed models of the human atrial action potential. Our objectives were to gain insight into the comparative mechanisms of each model by first calculating variance based sensitivity indices that quantify how variance in model inputs influences variance in model outputs, and second by examining how each model behaved under uncertain inputs.

Materials and methods

Human atrial cell models.

Several models of the human atrial action potential have been developed and are reviewed in detail elsewhere [6, 7, 12]. We selected two models for the present study, both based on data from human atrial cells. The first model is the *Courtemanche* model [20]. The second model is an extension of the model developed by Nygren et al [21], with modifications to the I_{Kur} and I_{to} currents as well as the movement of Na^+ [22], which we refer to as the *Maleckar* model.

We chose these models because both represent the action potential of human atrial cells, and so have clinical relevance. Both have been used for tissue and whole-organ scale simulations of atrial fibrillation [23–26]. Furthermore, both models have a comparable set of ion channels, pumps, and exchangers, however differences in Ca^{2+} handling underlie the different action potential shapes [7].

Model inputs and outputs

The Courtemanche and Maleckar cell models include components that represent membrane electrophysiology as well as intracellular Ca^{2+} storage, uptake, and release. We chose to concentrate on parameters that control the maximum current density carried by ion channels, pumps, and exchangers in the cell membrane as well as those that control the rate and magnitude of uptake and release of intracellular Ca^{2+}. We also selected the cell capacitance C_m, and the extracellular concentrations $[Na^+]_o$, $[K^+]_o$, and $[Ca^{2+}]_o$ as additional inputs. The inputs examined in this study are listed in Table 1, where the central values given are the default for each model.

The rationale for this choice was that each of the selected inputs can be considered uncertain (*i.e.* not a physical constant), yet has a biophysical interpretation. Maximum conductances of ion channels, pumps, and exchangers depend on protein expression, and so could be expected to vary within an individual cell at different times as well as from cell to cell. Cell size and capacitance vary from cell to cell. This natural variability can be considered to be aleatoric uncertainty, which is irreducible [16]. On the other hand, the kinetics of transmembrane currents are related to ion channel biophysics, and so could be considered epistemic uncertainty, which can in principle be reduced.

bioRxiv preprint doi: https://doi.org/10.1101/818047; this version posted October 24, 2019. The copyright holder for this preprint (which was not certified by peer review) is the author/funder, who has granted bioRxiv a license to display the preprint in perpetuity. It is made available under aCC-BY 4.0 International license.

Our analysis proceeded in two stages. In *Stage 1* the influence of all of the inputs listed in Table 1 was examined for a fixed pacing cycle length of 1000 ms. In *Stage 2*, a subset of the inputs was selected on the basis of their *Stage 1* sensitivity index (see below), and a new set of emulators was built using this subset as inputs, together with the diastolic interval (DI) of the S2 beat in an S1-S2 pacing sequence as an additional input.

Cardiac cell models produce an output that is a time series of states. Of these, membrane voltage V_m and intracellular Ca^{2+} concentration $[Ca^{2+}]_i$ describe the time course of action potentials and Ca^{2+}. To investigate how cell model inputs influence action potential shape, we selected nine features of the action potential that quantify its shape, based on biomarkers used in related work [11,12] as well as the minimum and maximum intracellular Ca^{2+} concentration. These eleven outputs are shown in Fig 1 and are listed below.

- dV_m/dt_{max} – Maximum slope of the action potential upstroke.
- V_{max} – Peak voltage of the action potential.
- V_{20}, V_{40}, V_{60}, and V_{80} – Membrane voltage measured at 20, 40, 60, and 80% of APD_{90}.
- APD_{50} and APD_{90} – Action potential duration at 50% and 90% of repolarisation.
- $RestV_m$ – Resting membrane potential, calculated as the average membrane voltage over a 10 ms period, 100 ms prior to the action potential upstroke.
- Ca^{2+}_{min} and Ca^{2+}_{max} – Minimum and maximum intracellular Ca^{2+} concentration.

Fig 1. Action potential biomarkers Nine action potential biomarkers were used as outputs to characterise each simulator run. A: Courtemanche model, B: Maleckar model. Biomarker labels are a: dV/dt_{max}, b: V_{max}, c-f: V_{20}, V_{40}, V_{60}, and V_{80}, g: APD_{50}, h: APD_{90}, i: $RestV_m$. Ca^{2+}_{max} and Ca^{2+}_{min} not shown

Model implementation

Both cell models were implemented in Matlab (Mathworks inc.), using Matlab code automatically generated from the CellML repository (`http://cellml.org`). The models were solved using the `ode15s` time adaptive solver for stiff systems of ODEs with the relative and absolute tolerance both set to 10^{-6}, and the maximum time step set to 0.5 ms.

To ensure that both cell models remained stable over the range of inputs used to train the GP emulators, we made some small modifications. Previous studies (for example [6]) have identified an instability in the Courtemanche model that arises from a gradual drift in the intracellular concentrations $[\mathrm{Na}^+]_\mathrm{i}$ and $[K^+]_i$. We therefore fixed $[Na^+]_i$ and $[K^+]_i$ at their default initial values of 11.17 and 139.00 mM respectively in the Courtemanche model implementation. In the Maleckar model, we fixed the $I_{K,Ach}$ current to zero.

For each run, action potentials were initiated by an inward current of 2000 pA delivered for 2 ms in the Courtemanche model, and $750/\mathrm{C_m}$ pA/pF for 6 ms in the Maleckar model. In *Stage 1*, each run comprised 40 action potentials at a cycle length of 1000 ms. In *Stage 2*, each run was composed of 39 S1 action potentials at a cycle length of 1000 ms and a final S2 stimulus delivered at an S1S2 interval determined by the $\mathrm{APD_{90}}$ of the final S1 beat, plus an offset of 10 ms, plus a diastolic interval (DI) with a

bioRxiv preprint doi: https://doi.org/10.1101/818047; this version posted October 24, 2019. The copyright holder for this preprint (which was not certified by peer review) is the author/funder, who has granted bioRxiv a license to display the preprint in perpetuity. It is made available under aCC-BY 4.0 International license.

range of 50-450 ms sampled using a Latin hyper-cube design with the other selected inputs as described below.

Gaussian process emulators

Our overall approach is described in detail in a previous paper [18]. We treat the cardiac cell models as simulators which produce a vector of model outputs $\mathbf{y_s}$ as a function of a vector of model inputs (parameters) $\mathbf{x}$ such that $\mathbf{y_s} = f_s(\mathbf{x})$. An emulator is then a statistical model of the simulator, sometimes known as a meta-model, a surrogate model, or a response surface model. The emulator approximates the model as $\mathbf{y_e} = f_e(\mathbf{x})$, where the emulator output approximates the simulator output $\mathbf{y_e} \approx \mathbf{y_s}$ for a given input $\mathbf{x}$.

In the present study we specified the emulator as a Gaussian process (GP), where the GP hyperparameters are optimized using a set of simulator runs called *design data*. When the GP has been fitted, the posterior prediction $\mathbf{y_e}$ at an input $\mathbf{x}^*$ can be evaluated, which is a probability density with an expectation and a variance. The variance for the prediction $\mathbf{y_e}$ expresses uncertainty in the prediction of the simulator behaviour at $\mathbf{x}^*$ [27, 28].

Simulator runs for emulator design data

For *Stage 1* we generated design data from 300 runs of each cell model implemented as described above. The inputs for this design were sampled using an optimized Latin hyper-cube design ranging from ±50% of the central values (model defaults) given in Table 1 (i.e. from central value ×0.5 to central value ×1.5), except for G_{K1}, C_m, and extracellular ion concentrations. To reduce the incidence of instability (see below), these inputs had ranges of ±25%, ±25%, and ±10% respectively. A set of output biomarkers was obtained from the final action potential. A further set of 150 model model runs were then used for emulator validation (see below). For *Stage 2*, a second set of design data was produced from 200 simulator runs of each model, with a reduced set of inputs sampled from a Latin hyper-cube as described in the results section, and other inputs set to their central value. A further set of 100 simulator runs were used for emulator validation.

Fig 2. Design data Action potentials and calcium transients produced by Latin hyper-cube sampling as described in the main text, and running each model with a pacing cycle length of 1000 ms. Traces shown in grey were used for emulator design data, and those shown in blue were excluded (see text for details). A, B: Courtemanche model. C, D: Maleckar model.

Outputs from the model runs used for *Stage 1* design data in the Courtemanche model and Maleckar model are shown in Fig 2. A wide variation in action potential shapes and durations were elicited by varying the model inputs.

Model runs were removed from the design data if there was instability or abnormality in the model outputs evidenced by pacemaking activity, a resting potential greater than -60 mV, APD_{90} greater than 600 ms, or if APD_{90} of the 39th and 40th beats differed by more than 5% indicating alternans. Using these criteria, 5 out of 300 Courtemanche model runs in *Stage 1* were removed, because of a long APD or APD alternans. In the Maleckar model 14 out of 300 model runs in *Stage 1* were removed, all with pacemaking activity or failure to repolarise. In Fig 2 the removed runs are highlighted in blue. In *Stage 2* no model runs were removed for the Courtemenache model, and 5 model runs were removed for the Maleckar model.

bioRxiv preprint doi: https://doi.org/10.1101/818047; this version posted October 24, 2019. The copyright holder for this preprint (which was not certified by peer review) is the author/funder, who has granted bioRxiv a license to display the preprint in perpetuity. It is made available under aCC-BY 4.0 International license.

Table 1. Range of inputs used for design data in each cell model.

Courtemanche model			
Input	Central value	Range	Units
G_{Na}	7.8	5.85 - 11.70 (±50%)	nS/pF
G_{K1}	0.09	0.045 - 0.018 (±25%)	nS/pF
G_{to}	0.165	0.0826 - 0.0330 (±50%)	nS/pF
fG_{Kur}	1.0	0.50 - 1.50 (±50%)	none
G_{Kr}	0.0294	0.0147 - 0.0441 (±50%)	nS/pF
G_{Ks}	0.1294	0.0647 - 0.1941 (±50%)	nS/pF
$G_{Ca,L}$	0.1237	0.0619 - 0.1856 (±50%)	nS/pF
$G_{b,Na}$	0.0006	0.0003 - 0.0010 (±50%)	nS/pF
$G_{b,Ca}$	0.0011	0.0005 - 0.0017 (±50%)	nS/pF
$i_{NaK}Max$	0.5993	0.2997 - 0.8990 (±50%)	pA/pF
$i_{NaCa}Max$	1600.0	800.00- 2400.0 (±50%)	pA/pF
$i_{p,Ca}Max$	0.275	0.1375 - 0.4125 (±50%)	pA/pF
K_{rel}	0.30	0.15 - 0.45 (±50%)	/ms
τ_{tr}	180.0	90.0 - 270.0 (±50%)	ms
$i_{up}Max$	0.005	0.0025 - 0.0075 (±50%)	mM/ms
K_{up}	0.00092	0.00046 - 0.0014 ±50%)	mM
C_m	100.0	75.0 - 125.0 (±25%)	pF
$[Na^+]_o$	140.0	126.0 - 154.0 (±10%)	mM
$[K^+]_o$	5.4	4.86 - 5.94 (±10%)	mM
$[Ca^{2+}]_o$	1.8	1.62 - 1.98 (±10%)	mM

Maleckar model			
Input	Central value	Range	Units
P_{Na}	0.0018	0.0009 - 0.0027 (±50%)	nL/s
G_{K1}	3.1	2.325 - 3.875 (±25%)	nS
G_t	8.25	4.125 - 12.375 (±50%)	nS
G_{Kur}	2.25	1.125 - 3.375 (±50%)	nS
G_{Kr}	0.5	0.250 - 0.750 (±50%)	nS
G_{Ks}	1.0	0.50 - 1.50 (±50%)	nS
$G_{Ca,L}$	6.75	3.375 - 10.125 (±50%)	nS
$G_{b,Na}$	0.0605	0.303 - 0.909 (±50%)	nS
$G_{b,Ca}$	0.0590	0.0295 - 0.0885 (±50%)	nS
$NaKMax$	68.55	34.27 - 102.82 (±50%)	pA
K_{NaCa}	0.0750	0.0375 - 0.1125 (±50%)	pA/mM^4
$i_{p,Ca}Max$	4.0	2.0 - 6.0 (±50%)	pA
α_{rel}	200000	100000 - 300000 (±50%)	pA/mM
τ_{tr}	0.01	0.005 - 0.015 (±50%)	s
$i_{up}Max$	2800	1400 - 4300 (±50%)	pA
K_{cyca}	0.0003	0.00015 - 0.00045 (±50%)	mM
K_{srca}	0.5	0.25 - 0.75 (±50%)	mM
K_{xcs}	0.4	0.2 - 0.6 (±50%)	dimensionless
C_m	50	37.5 - 62.5 (±25%)	pF
$[Na^+]_o$	140.0	126.0 - 154.0 (±10%)	mM
$[K^+]_o$	5.4	4.86 - 5.94 (±10%)	mM
$[Ca^{2+}]_o$	1.8	1.62 - 1.98 (±10%)	mM

bioRxiv preprint doi: https://doi.org/10.1101/818047; this version posted October 24, 2019. The copyright holder for this preprint (which was not certified by peer review) is the author/funder, who has granted bioRxiv a license to display the preprint in perpetuity. It is made available under aCC-BY 4.0 International license.

Emulator fitting.

Our approach to fitting and using GP emulators is described in full detail elsewhere [18, 19]. Mathematical details including the expression for the posterior prediction of the emulator are provided in Supporting Information as well as in [27–29], and the Python code used in this study for emulator fitting, validation, sensitivity and uncertainty analysis is available from `https://github.com/samcoveney/maGPy`. Briefly, each emulator was composed of a mean function and a zero mean Gaussian Process,

$$f_e(\mathbf{x}) = m(\mathbf{x}) + g(\mathbf{x}); \tag{1}$$

with a linear mean,

$$m(\mathbf{x}) = h(\mathbf{x})^T\beta = \beta_0 + \beta_1 x_1 + ... + \beta_P x_P, \tag{2}$$

and a zero-mean GP,

$$g(\mathbf{x}) \sim \mathcal{GP}(0, \sigma^2 c(\mathbf{x}, \mathbf{x}')), \tag{3}$$

where the covariance has a Radial Basis Function form,

$$c(\mathbf{x}, \mathbf{x}') = \exp\left[-\sum_{p=1}^{P} \frac{\left(x_p - x_p'\right)^2}{\delta_p^2}\right]. \tag{4}$$

In these expressions $\mathbf{x} = (x_1, x_2, \ ... \ , x_P)$ are the P inputs (parameters), the emulator hyperparameters β and δ are vectors of length P, and σ^2 is a scalar. The hyperparameters were obtained by maximum log-likelihood fitting to model inputs and outputs in the design data, assuming weak prior information on β and σ^2 [29], and with a fixed nugget of 10^{-7} [30]. To avoid the fitting process becoming trapped in a local maximum, we repeated each fit ten times, each with a different set of randomly chosen initial values for the hyperparameters. The fit with the greatest log-likelihood was then selected. We produced a separate emulator for each of the outputs shown in Fig 1.

Sensitivity and uncertainty analysis

Sensitivity and uncertainty analysis can be seen as distinct but related topics; where sensitivity analysis identifies the contribution of variance in each input to variance in each output, and uncertainty analysis concentrates on estimating the uncertainty in model outputs [31].

We calculated a first order sensitivity index for each combination of input and output [28]. For each input i, the first order sensitivity index describes how much the output variance would be reduced if x_i is fixed, while all other inputs are uncertain. The first order index is expressed as a proportion of the output variance calculated when all inputs are considered uncertain.

$$S_w = \frac{Var[E(f_e(\mathbf{x}|x_w))]}{Var[f_e(\mathbf{x})]} \tag{5}$$

To capture the effect of interactions between the inputs, the total effect index can be calculated. This describes the reduction in output variance when x_w is uncertain and all other inputs are fixed, denoted as $x_{\sim w}$. It is also expressed as a proportion of the output variance when all inputs are considered uncertain.

$$S_{Tw} = \frac{Var[f_e(\mathbf{x})] - Var[f_e(\mathbf{x}|x_{\sim w})]}{Var[f_e(\mathbf{x})]} \tag{6}$$

bioRxiv preprint doi: https://doi.org/10.1101/818047; this version posted October 24, 2019. The copyright holder for this preprint (which was not certified by peer review) is the author/funder, who has granted bioRxiv a license to display the preprint in perpetuity. It is made available under aCC-BY 4.0 International license.

The difference between S_{Tw} and S_w is then the contribution of all interactions between x_w and $x_{\sim w}$ to the variance in the output. These quantities were calculated using expressions given in the Supporting Information and described in [28]. Each uncertain input was assigned a mean of 0.5 in normalised units defined by the input ranges given in Table 1. Inputs that varied ±50% were assigned a variance of 0.02, G_{K1} and C_m were assigned a variance of 0.04, and the extracellular ionic concentrations were assigned a variance of 0.1. We also calculated the main effect of each input on each output, using the procedure described in the Supporting Information, and the gradient of the main effect of a particular input around 0.5 normalised units was used to allocate a sign to the corresponding first order sensitivity index.

Several recent studies have calculated sensitivity indices based on partial least squares (PLS) regression [32, 33]. In this approach, each model output is assumed to be a weighted sum of inputs. Thus the model is described by the linear relationship

$$\mathbf{y} = \mathbf{xB}, \tag{7}$$

where $\mathbf{y} = (y_1, y_2, \ldots, y_M)$ is a vector of M outputs, $\mathbf{x} = (x_1, x_2, \ldots, x_P)$ a vector of P inputs, and $\mathbf{B}$ a $P \times M$ matrix of regression coefficients. An estimate of the matrix $\mathbf{B}$, $\mathbf{B_{PLS}}$, can be found by PLS regression on a set of design data obtained from N model runs, that generates an $N \times M$ matrix of inputs $\mathbf{Y}$ and an $N \times P$ matrix of outputs $\mathbf{X}$. Each element of $\mathbf{X}, x_{i,j}$ is regularised by subtracting the mean $\overline{x_j}$ and dividing by the standard deviation of x_j, and each element of $\mathbf{Y}$ is regularised in the same way. $\mathbf{B_{PLS}}$ is found by minimising the difference $||\hat{\mathbf{Y}} - \mathbf{Y}||$, where $\hat{\mathbf{Y}} = \mathbf{XB_{PLS}}$.

The matrix $\mathbf{B_{PLS}}$ can be interpreted as a matrix of sensitivity indices, provided the linear model holds. Each element of $\mathbf{B_{PLS}}$, $b_{i,j}$ describes how changing input x_i results in a corresponding change in output y_j. In both cases the change is relative to the mean value, and is a fraction of its standard deviation.

For comparison with variance based sensitivity indices, we calculated PLS sensitivity indices from the *Stage 1* design data used to train the GP emulators. The input and output matrices $\mathbf{X}$ and $\mathbf{Y}$ were constructed from regularised design data inputs and outputs. The regression matrix $\mathbf{B_{PLS}}$ was then calculated using the Matlab function `mvregress`.

Emulator validation.

Each emulator was validated against an independent set of 150 simulator runs for *Stage 1* and 100 simulator runs for *Stage 2*. For each output, we calculated the mean average predicted error (MAPE) and the median individual standard error (ISE) for each validation run. The MAPE was given by

$$MAPE = \frac{100\%}{N} \frac{1}{\overline{y_s}} \sum_{n=1}^{N} |y_s^n - y_e^n|, \tag{8}$$

where N was the number of validation runs, y_s^n simulator output for run n, and y_e^n the posterior mean emulator output for run n. We used the mean of the simulator output $\overline{y_s}$ as a denominator instead of $|y_s^n|$ to avoid bias associated with small values of $|y_s^n|$.

$$ISE = \frac{|y_s^n - y_e^n|}{\sqrt{Var(n,n)}}, \tag{9}$$

where y_s^n was the simulator output for run n, y_e^n the posterior mean emulator output for run n, and $Var(n,n)$ the posterior emulator variance for run n.

For most stage *Stage 1* and *Stage 2* emulators the MAPE was less than 10% and the median ISE was less than 1.0. Most of the differences between the output from the

bioRxiv preprint doi: https://doi.org/10.1101/818047; this version posted October 24, 2019. The copyright holder for this preprint (which was not certified by peer review) is the author/funder, who has granted bioRxiv a license to display the preprint in perpetuity. It is made available under aCC-BY 4.0 International license.

emulator and the output of the simulator for a given set of inputs were small, and so the fit of the emulators was considered acceptable. A Table of MAPE and ISE is provided in the Supporting Information.

Results

Stage 1 sensitivity indices

The first order sensitivity indices for both cell models are shown in Fig 3. Each row of the figure corresponds to one of the model outputs, and each column represents a model output. The sign of each sensitivity index was determined from the slope of the main effect (see below). The sum of the absolute values of the sensitivity indices for each output is given to the right of each grid. Since first order sensitivity indices are a proportion, a sum close to one indicates that almost all of the output variance is accounted for by the variance on each input. Smaller values for this sum, such as those for APD_{50} and APD_{90}, can indicate that there are interactions among the inputs.

Fig 3. *Stage 1* first order sensitivity indices. The first order sensitivity index for each input and output is given, with a sign based on the gradient of the mean effect. Sensitivity indices less than 0.05 not shown, to assist visualization. The numbers at the right hand side of the table indicate the sum of the absolute values of sensitivity indices along each row. A: Courtemanche model. B: Maleckar model.

The total effect indices are shown in Fig 4. For each combination of input and output, the difference between the total effect index and the first order index reflects interactions with the other inputs. The sum of these differences is shown at the right hand side of Fig 4. In most cases the first order and total effect indices are similar, and the sum of differences is small indicating that the effect of interactions is small. However, the sum of differences is larger for V_{80} in the Courtemanche model, as well as for APD_{50} and APD_{90} in both models, and we conclude that there are interactions between inputs, and these interactions have an effect on repolarisation.

Fig 4. *Stage 1* total effect indices. The total effect sensitivity index for each input and output is given, indices less than 0.01 not shown. Numbers on right hand side are the the sum across each row of the differences between the total effect index and the absolute value of the first order index. A: Courtemanche model. B: Maleckar model.

For comparison, Fig 5 shows sensitivity indices obtained by PLS regression on the emulator design data, and a comparison with variance based first order indices. The comparison plots show broad agreement, with the first order indices $S_i \approx B_i^2$. This relationship arises from the different definitions of S_i and B_i based on variance and standard deviation respectively [34].

Fig 5. Multivariate regression sensitivity indices. The sensitivity index based on multivariate regression for each input and output is given. Right hand panels compare these sensitivity indices with those obtained from GP regression and shown in Fig 3. A: Courtemanche model. B: Maleckar model.

Overall these sensitivity indices show the contribution of uncertainty in each input to uncertainty in each output. Thus the main contributors to uncertainty in dV/dt_{max} are the Na^+ channel maximum conductances G_{Na} and P_{Na}, and the membrane capacitance C_m. The sign of the sensitivity indices show that these act in opposite

bioRxiv preprint doi: https://doi.org/10.1101/818047; this version posted October 24, 2019. The copyright holder for this preprint (which was not certified by peer review) is the author/funder, who has granted bioRxiv a license to display the preprint in perpetuity. It is made available under aCC-BY 4.0 International license.

directions, as would be expected from the role played by the Na^+ current in depolarisation: increasing Na^+ current acts to increase dV/dt_{max}, whereas increasing C_m acts to decrease dV/dt_{max}. The bigger influence of C_m in the Maleckar model arises becuase the stimulus current scales with $1/C_m$; a larger C_m results in a smaller stimulus current, which in turn produces a smaller dV/dt_{max} and a smaller V_{max}.

In both models, these sensitivity indices can be interpreted to show that increased outward currents (such as G_{Kur}) act to decrease both the voltage of the action potential plateau and action potential duration, whereas increased outward currents G_{GaL} and G_{bCa} have an opposite effect. In the Maleckar model $I_{NaK}Max$ has the opposite effect to G_{bCa}. In the Courtemanche model, Ca^{2+}_{max} and Ca^{2+}_{min} are influenced by G_{CaL}, G_{bCa}, $I_{NaCaMax}$ and Ca^{2+} handling parameters I_{rel} and K_{up}, whereas in the Maleckar model G_{CaL} and K_{NaCa} have a negligible effect, and this reflects the different formulation of Ca^{2+} handling in the two models [7].

The sensitivity analysis shows that several inputs influence APD_{50}, APD_{90}, $RestV_m$, and Ca^{2+}_{max}. Fig 6 shows the main effect of each input on these outputs, for each cell model. The main effect shows the expected value of the output as each input is fixed and varied in turn across the normalised range $0 \ldots 1$ corresponding to the input ranges given in Table 1, while all other inputs are considered uncertain. The residual variance arising from the uncertain inputs accounts for the fact that the main effects do not converge exactly for an input value of 0.5.

Fig 6. Stage 1 selected main effects plots. Main effects for APD_{50}, APD_{90}, $RestV_m$, and Ca^{2+}_{max}. A: Courtemanche model. B: Maleckar model.

Some of the effects are comparable between the two models, for example increasing G_{bCa} acts to increase APD_{90}, $RestV_m$, and Ca^{2+}_{max}. Several of the effects are nonlinear, for example the main effect of G_{CaL} on APD_{50} and APD_{90}. However, the overall picture is complex, and it is hard to compare the different models. In order to simplify the analysis, we selected a subset of inputs for *Stage 2* of the analysis based on their sensitivity indices as described below.

Stage 2 sensitivity analysis

For *Stage 2*, we concentrated on inputs that strongly influenced action potential shape and duration, with first order sensitivity index of more than 0.1. To simplify the analysis further, we excluded G_{Na} and P_{Na} as these inputs mainly influence action potential upstroke and amplitude. We also excluded extracellular concentrations, since these are tightly controlled in normal physiological conditions, and we excluded the inputs directly involved in the storage, uptake and release of intracellular Ca^{2+} because we sought to concentrate on action potential shape and duration. The *Stage 2* inputs selected for the Courtemanche model were G_{K1}, G_{to}, $G_{KurMult}$, G_{CaL}, G_{bCa}, $I_{NaK}Max$, $I_{NaCa}Max$, and $I_{PCa}Max$, and for the Maleckar model G_{K1}, G_t, G_{Kur}, G_{CaL}, G_{bCa}, $I_{NaK}Max$, and C_m. All other inputs were assigned their central value from Table 1. In addition, the DI of the final action potential was introduced as an additional input to explore the dynamic behaviour of the model.

The sensitivity indices for *Stage 2* are shown in Fig 7 and 8, and the main effects for APD_{50}, APD_{90}, $RestV_m$, and Ca^{2+}_{max} in Fig 9.

Overall, both first order and total effect sensitivity indices were similar to *Stage 1*, but the interactions for the Courtemanche model were larger than for *Stage 1*. In the Courtemanche model both first order and total effect indices for DI were larger than for the Maeckar model, indicating that DI acts to influence both the shape and duration of the action potential in the Courtemanche model.

bioRxiv preprint doi: https://doi.org/10.1101/818047; this version posted October 24, 2019. The copyright holder for this preprint (which was not certified by peer review) is the author/funder, who has granted bioRxiv a license to display the preprint in perpetuity. It is made available under aCC-BY 4.0 International license.

Fig 7. *Stage 2* first order sensitivity indices. The first order sensitivity index for each input and output is given, with a sign based on the gradient of the mean effect. Sensitivity indices less than 0.05 not shown. The numbers at the right hand side of the table indicate the sum of sensitivity indices along each row. A: Courtemanche model. B: Maleckar model.

Fig 8. *Stage 2* total effect sensitivity indices. The total effect index for each input and output is given, indices less than 0.01 not shown. A: Courtemanche model. B: Maleckar model.

Fig 9. *Stage 2* selected main effects plots. Stage 2 main effects for APD_{50}, APD_{90}, $RestV_m$, and Ca^{2+}_{max}. A: Courtemanche model. B: Maleckar model.

The main effects plots show opposite effects of inward and outward currents on action potential duration; however APD_{50} as a proportion of APD_{90} in the Maleckar model was considerably shorter than in the Courtemanche model as a result of the different action potential shape, and so both the sensitivity indices and main effects for APD_{50} may not be easily comparable. This observation is reflected in the larger main effect of DI on APD_{50} in the Courtemanche model. The main effects plots also show several nonlinear relationships, for example the main effect of G_{Kur} was nonlinear in each of the outputs shown in Fig 9. The main effect of G_{Kur} on APD_{90} in the Maleckar model was larger, and in an opposite direction, to the main effect in the Courtemanche model. This was explored in additional simulations where G_{Kur} was decreased to 50% and increased to 150% of its default value. Fig 10 shows a simulated action potential, together with the principal inward and outward currents that act during the action potential plateau.

Fig 10. Effect of magnitude of I_{Kur} on inward and outward currents. Simulated action potential, outward current I_{Kur}, inward current $I_{Ca,L}$, and outward current I_{Kr}. In each case the final beat of 40 is shown, with a pacing cycle length of 1000 ms. A: Courtemanche model. B: Maleckar model.

Changing G_{Kur} influenced the voltage of the action potential plateau in both models, but had a different effect on the timing of repolarisation because of different current formulations in each model. The time course of I_{to} in both models was similar, and was not strongly influenced by G_{Kur} and so is not shown. A decrease in G_{Kur} reduced the outward current during the initial part of the action potential plateau. This resulted in an increased voltage during the plateau, and a larger inward $I_{Ca,L}$, which is voltage-dependent and acts to prolong the action potential plateau. In turn, the increased plateau voltage resulted in greater activation of the outward current I_{Kr}, which is larger in the Courtemanche model compared to the Maleckar model. Thus in the Courtemanche model, a decrease in G_{Kur} resulted in increased I_{Kr}, with little change in action potential duration. In the Maleckar model I_{Kr} is much smaller, and so the increased plateau voltage did not result in increased outward current during repolarisation, and so action potential duration was prolonged.

APD restitution

The *Stage 2* analysis included diastolic interval as an input, which enabled us use the emulators to examine how different inputs affect APD restitution. In Fig 11 we have plotted a surface showing the expected value of APD_{90}, coloured by the 95% credible interval (see Supporting Information). In each of these plots the emulators were

bioRxiv preprint doi: https://doi.org/10.1101/818047; this version posted October 24, 2019. The copyright holder for this preprint (which was not certified by peer review) is the author/funder, who has granted bioRxiv a license to display the preprint in perpetuity. It is made available under aCC-BY 4.0 International license.

evaluated with all inputs assigned fixed values with no uncertainty, and so the 95% credible intervals reflect only uncertainty in the emulator fit, with no uncertainty arising from uncertainty in the inputs. We assigned a value of 0.5 in normalised units to all of the inputs, except for DI and another inputs that were varied in each plot; these were assigned fixed values between $0 \ldots 1$.

Fig 11. APD_{90} as a function of DI and other inputs. Each plot shows a surface of predicted mean APD_{90}, coloured by the 95% credible interval. A: Courtemanche model. B: Maleckar model.

Overall, APD_{90} restitution was flatter in the Maleckar model compared to the Courtemanche model, which is consistent with other studies [6,7]. The overall effect of G_{K1}, G_{CaL} and G_{bCa} on APD_{90} was similar in each model, with I_{NaKax} in the Courtemanche model having a similar effect to G_{Kur} in the Maleckar model.

However the shape of the APD_{90} restitution was modulated to some extent by the other inputs shown. In the Courtemanche model, decreasing G_{bCa} resulted in steepening of APD_{90} restitution, with a marked decrease in APD_{90} for short DI as G_{bCa} was changed from 150% to 50% of its central value. The Maleckar model also showed a marked decrease in APD_{90} as G_{bCa} was reduced, but this change was seen across the full range of DI.

Uncertainty analysis

We assessed how the uncertainty in model outputs changed as uncertainty in all of the model inputs was increased, and the results for APD_{90} are shown in Fig 12. Uncertainty in APD_{90} increased monotonically with uncertainty in the inputs, for both *Stage 1* and *Stage 2*. Reducing the number of uncertain inputs for *Stage 2* acted to reduce the output uncertainty for the Maleckar model, but increased output uncertainty slightly in the Courtemanche model. This rather unexpected finding may be due to interactions among the inputs. However, in the Maleckar model, the total effects for APD_{90} in Fig4B are higher than the total effects for the Courtemanche model, indicating a greater degree of interaction in the Maleckar than Courtemanche models. The smaller number of inputs for *Stage 2* could then result in less uncertainty arising from interactions among uncertain inputs for the Maleckar model, and a consequent reduction in uncertainty. However fixing some inputs for the *Stage 2* analysis may have had an effect on interactions the in the Courtemanche model, leading to an increase in uncertainty in predicted APD_{90}. An alternative explanation would be that with some of the inputs fixed, the uncertain inputs contribute mote to output uncertainty in the Courtemanche model.

The first two bars of Fig 12C show the coefficient of variation for APD_{90} with inputs set to a mean of 0.5 and standard deviation of 0.1 in normalised units, corresponding to a single point for each model in Fig 12 A and B. The third set of bars (denoted Fix 1) show the coefficient of variation for APD_{90} when the three inputs with the highest sensitivity indices are fixed at 0.5, and the fourth set of bars (denoted Fix 2) show the coefficient of variation when all inputs except these three inputs are fixed at 0.5.

Discussion

In this study we have obtained novel insights into the comparative mechanisms of two atrial cell models, and have demonstrated the use of Gaussian process emulators for sensitivity and uncertainty analysis.

bioRxiv preprint doi: https://doi.org/10.1101/818047; this version posted October 24, 2019. The copyright holder for this preprint (which was not certified by peer review) is the author/funder, who has granted bioRxiv a license to display the preprint in perpetuity. It is made available under aCC-BY 4.0 International license.

Fig 12. Uncertainty in APD_{90} and V_{max} Coefficient of variation (standard deviation divided by mean) in APD_{90} for *Stage 1* (A) and *Stage 2* plotted against imposed uncertainty on all inputs (B) for each model, with different mean values of 0.4, 0.5, and 0.6 in normalised units. (C) Coefficient of variation in APD_{90} for *Stage 1*; *Stage 2*; simulations where G_{K1}, G_{Kr} (G_{Kur} for Maleckar model), and G_{bCa} were fixed at 0.5 and all other inputs were uncertain with standard deviation of 0.1 (Fix 1); and simulations where all other inputs were fixed with mean of 0.5, and G_{K1}, G_{Kr} (G_{Kur} for Maleckar model), and G_{bCa} were uncertain with standard deviation of 0.1.

Human atrial cell models

Models of the human atrial action potential are a subject of research interest and clinical relevance because heterogeneity in action potential shape and duration in different parts of the atria is associated with vulnerability to atrial fibrillation [35], and persistence of atrial fibrillation is associated with remodelling of the atrial action potential [23, 36]. There are several different models of human atrial myocytes, each with different properties [6, 7, 37]. Most studies of these models have focussed on the mechanisms that change action potential duration because a reduced APD increases vulnerability to atrial fibrillation, and APD can be modulated pharmacologically [7, 9, 12, 21, 38]. These previous studies have highlighted the importance of I_{CaL}, as well as I_{K1} and I_{Kur}, in regulating APD. The present study adds to our understanding of the Courtemanche and Maleckar models by providing a more comprehensive view of how the model parameters affect the shape and duration of the action potential, as well as the maximum and minimum of the Ca^{2+} transient.

Increased inward current tends to increase amplitude of the upstroke and plateau as well as increasing APD, and increased outward current tends to have the opposite effect. The present study has highlighted how action potential duration and shape depends on the net flow of charge across the cell membrane, which is finely balanced so small changes in the magnitudes of inward and outward currents can strongly influence action potential shape and duration. The two models examined in this study represent repolarisation using a different balance of currents, and this difference along with the consequences can be seen in Fig 10. The relative magnitudes of I_{CaL} and I_{Kr} in the two models are different, with much smaller I_{CaL} and I_{Kr} in the Maleckar model. This may explain why G_{bCa} exerts a stronger influence over $Ca_m^{2+}in$ and $Ca_m^{2+}ax$ in the Maleckar model compared to the Courtemanche model.

Overall, the difference between the first order sensitivity indices (Fig 3) and the total effect indices (Fig 4) was small. The sum of these differences for each output (right hand column in Fig 4 and Fig 8) indicates more interactions in the Courtemanche model than in the Maleckar model, and that these interactions tend to affect the plateau of the action potential. These observations mean that overall the interactions between the inputs in these models do not have a strong effect on the outputs, and so we can conclude that the inputs examined in this study tend to act independently. This is a potentially important feature of the models, which could be exploited for model calibration as well as for examining mechanisms of remodelling and pharmacological action. However, it remains to be seen whether this independence is a feature of real cardiac myocytes.

Sensitivity and uncertainty analysis

As models of cardiac cell and tissue electrophysiology become more widely used, it is becoming increasingly important to understand how different components of the models influence model behaviour, and especially how these different components interact.

bioRxiv preprint doi: https://doi.org/10.1101/818047; this version posted October 24, 2019. The copyright holder for this preprint (which was not certified by peer review) is the author/funder, who has granted bioRxiv a license to display the preprint in perpetuity. It is made available under aCC-BY 4.0 International license.

Biophysically detailed cardiac cell models are complex, with many interacting parts. Some of these model components may be inherited from earlier models and experiments [8], and the process by which model parameters are fitted is also fragile when there are uncertainties associated with experimental data [5]. The development and evaluation of tools for sensitivity and uncertainty analysis of cardiac models is therefore an important and growing area [16], but much remains to be done.

Several recent studies have pioneered the use sensitivity indices obtained by of partial least squares (PLS) regression of simulator outputs on simulator inputs, which allows a calculation of sensitivity indices [9, 10, 32]. This approach is straightforward to implement, and we have found that it gives sensitivity indices that agree well with the square root of the first order index obtained using the GP approach (Fig 5), and the reason for this appears to be that the PLS and GP indices are based on variance and standard deviation respectively. The overall agreement indicates that both approaches can yield similar first order sensitivity indices, although the GP easily enables calculation of interaction effects as well as first order indices. Other approaches for uncertainty and sensitivity analysis based on generalised polynomial chaos expansion have also been developed and used for analysis of cardiovascular system models [17]. These approaches also enable calculation of sensitivity indices, but the relative merits of these different approaches are only beginning to be explored [43]. Both GP emulators and polynomial chaos expansions enable the explicit treatment of uncertainties, and so offer advantages for more comprehensive model analysis.

Gaussian process emulation of biophysical models

The present study has focussed on Gaussian process (GP) emulators, which are one class of tools for sensitivity and uncertainty analysis. A GP acts to interpolate an output surface, providing a probabilistic estimate of a simulator output for a particular point in a high dimensional input space. A GP is quick to evaluate. It can be trained on a relatively small number of simulator runs, and so offers advantages over other approaches that rely on large numbers of simulator evaluations [12, 39].

A GP is usually trained using a set of design data composed of a set of simulator inputs and outputs. The emulator hyperparameters are obtained conditional on the design data using a maximum likelihood approach. The quality of the emulator fit can then be assessed by comparing the outputs obtained from the emulator for a particular set of inputs with those obtained by the simulator for the same set of inputs. In the present study we used the MAPE and ISE to quantify the difference between emulator and simulator outputs, although other measures such as the Mahanalobis distance can be used [18]. These measures provide some guidance about whether the emulator is under or over-fitted to the design data.

The number of simulator runs required to compose the design data remains an open question, and will depend on the complexity of the model output surfaces. A typical rule of thumb is to use ten times the number of inputs, and based on our previous experience [18] we opted for 300 runs for *Stage 1* and 200 runs for *Stage 2*. We also trained the *Stage 1* emulators on design data sets composed of 200 and 400 simulator runs, and obtained similar sensitivity indices to those presented here. However, further work is required to develop methods to determine the number of simulator runs needed as well as suitable metrics to determine emulator quality. One aspect of this challenge is to develop optimal sizes for design data and test data so that emulators can be trained and evaluated in a way that minimises the number of simulator runs and optimises the emulator fit.

Emulators should be trained on design data that fill the input space evenly, and we chose to use Latin hypercube sampling in this study [40]. Other methods, such as orthogonal sampling [41] may provide a better sampling strategy.

bioRxiv preprint doi: https://doi.org/10.1101/818047; this version posted October 24, 2019. The copyright holder for this preprint (which was not certified by peer review) is the author/funder, who has granted bioRxiv a license to display the preprint in perpetuity. It is made available under aCC-BY 4.0 International license.

The ability to evaluate emulators cheaply can be valuable for model calibration, where thorough exploration of a high dimensional input space is required [42]. A key benefit of a GP emulator approach is the explicit handling of uncertainty. Under the assumption that inputs and outputs have Gaussian distributions, the variance on the emulator output can be calculated directly, given variances on the inputs. This enables the direct calculation of sensitivity indices, as well as enabling a systematic investigation of the way that output uncertainties depend on uncertainties in the inputs.

Limitations, challenges and future directions

The use of emulators to probe detailed biophysical models is at an early stage, and so there are several limitations and challenges associated with the present study.

Choice of inputs

We concentrated on the effect of maximum conductances in the present study, as this reduced the complexity of the analysis. The rationale for this approach was an assumption that kinetic parameters are determined by biophysics, and so less prone to variation than the expression of ion channels, pumps, and exchangers. However, a detailed sensitivity analysis of I_{Kr} dynamics in the Courtemanche model showed that these kinetic parameters influence APD [44], and other studies have highlighted difficulties in calibrating ion channel dynamics using traditional approaches as well as showing that different formulations can have an important effect on the magnitude and time course of an ion channel current [45]. In the present study our focus was on the action potential rather than Ca^{2+} handling, and a detailed sensitivity analysis of the mechanisms of Ca^{2+} storage, release, and uptake in each model would be a valuable extension to the work presented here. So far a fully comprehensive analysis has only been done for specially constructed models [15]. Nevertheless, a complete sensitivity analysis of biophysically detailed models, possibly using a hierarchical approach, remains an important challenge.

Simulator instability

One of the issues with a complete sensitivity analysis, highlighted in [15], is that parts of the simulator input space may generate implausible behaviours. For a cardiac cell model these behaviours might be a numerical instability, spontaneous beats, or failure to repolarise. In the present study we removed simulator runs from the design data where model behaviour was implausible, or where the simulator runs produced action potential alternans. We considered this to be a pragmatic approach. However, it is clearly an area for improvement because the location of these regions of input space conveys information about the model, and approaches where these locations are encoded explicitly show promise [46].

Choice of outputs

We selected a range of action potential features for our model outputs, these were based on measures used to describe experimental action potentials and aim to capture the main features of the action potential shape and duration. Our main focus was on the action potential. We included the maximum and minimum intracellular Ca^{2+} concentration as additional outputs, but did not consider the duration of the Ca^{2+} transient. We would not consider our choice of outputs to be definitive, and there may be better choices. A principal component analysis of the design data used in the present study showed that 95% of the output variance was accounted for by the first 6 principal

bioRxiv preprint doi: https://doi.org/10.1101/818047; this version posted October 24, 2019. The copyright holder for this preprint (which was not certified by peer review) is the author/funder, who has granted bioRxiv a license to display the preprint in perpetuity. It is made available under aCC-BY 4.0 International license.

components for the Courtemanche model and the first 5 for the Maleckar model. Parameterising the action potential and Ca^{2+} transient so that they are described by a minimal set of features is likely to be important not only for model analysis but also for model calibration [42]. Emulators that emulate time-dependent outputs have been developed, but are not yet widely used [47, 48], but could be a promising tool for extending work in this area.

Future directions

Extending the use of emulators from models of cardiac cells to models of cardiac tissue is an important next step, and initial studies are promising [49]. At present, tissue calculations are computationally expensive, especially for personalised meshes. However, the need to evaluate uncertainty in model predictions for use in the clinical setting requires computationally efficient approaches, and we anticipate exciting developments in this area.

Supporting information

S1 Text Mathematical details. Details of the procedures used to fit and evaluate the Gaussian process emulators, and to calculate main effects and sensitivity indices.

References

1. Noble D. A modification of the Hodgkin—Huxley equations applicable to Purkinje fibre action and pacemaker potentials. Journal of Physiology (London). 1962;160(2):317–352.

2. Fink M, Niederer SA, Cherry EM, Fenton FH, Koivumaki JT, Seemann G, et al. Cardiac cell modelling: Observations from the heart of the cardiac physiome project. Progress in Biophysics and Molecular Biology. 2011;104:2–21.

3. Clayton RH, Bernus O, Cherry EM, Dierckx H, Fenton FH, Mirabella L, et al. Models of cardiac tissue electrophysiology: Progress, challenges and open questions. Progress in Biophysics and Molecular Biology. 2011;104(1-3):22–48. doi:10.1016/j.pbiomolbio.2010.05.008.

4. Hodgkin A, Huxley A. A quantitative description of membrane current and its application to conduction and excitation in nerve. Journal of Physiology (London). 1952;117:500–544.

5. Pathmanathan P, Shotwell MS, Gavaghan DJ, Cordeiro JM, Gray Ra. Uncertainty quantification of fast sodium current steady-state inactivation for multi-scale models of cardiac electrophysiology. Progress in Biophysics and Molecular Biology. 2015;117(1):1–15. doi:10.1016/j.pbiomolbio.2015.01.008.

6. Wilhelms M, Hettmann H, Maleckar MM, Koivumäki JT, Dössel O, Seemann G. Benchmarking electrophysiological models of human atrial myocytes. Frontiers in Physiology. 2012;3:487. doi:10.3389/fphys.2012.00487.

7. Cherry EM, Evans SJ. Properties of two human atrial cell models in tissue: restitution, memory, propagation, and reentry. Journal of Theoretical Biology. 2008;254:674–690.

bioRxiv preprint doi: https://doi.org/10.1101/818047; this version posted October 24, 2019. The copyright holder for this preprint (which was not certified by peer review) is the author/funder, who has granted bioRxiv a license to display the preprint in perpetuity. It is made available under aCC-BY 4.0 International license.

8. Niederer SA, Fink M, Noble D, Smith NP. A meta-analysis of cardiac electrophysiology computational models. Experimental Physiology. 2009;94(5):486–95. doi:10.1113/expphysiol.2008.044610.

9. Koivumäki JT, Seemann G, Maleckar MM, Tavi P. In Silico Screening of the Key Cellular Remodeling Targets in Chronic Atrial Fibrillation. PLoS Computational Biology. 2014;10(5):e1003620. doi:10.1371/journal.pcbi.1003620.

10. Sarkar AX, Christini DJ, Sobie Ea. Exploiting mathematical models to illuminate electrophysiological variability between individuals. Journal of Physiology (London). 2012;590(Pt 11):2555–67. doi:10.1113/jphysiol.2011.223313.

11. Britton OJ, Bueno-Orovio A, Van Ammel K, Lu HR, Towart R, Gallacher DJ, et al. Experimentally calibrated population of models predicts and explains intersubject variability in cardiac cellular electrophysiology. Proceedings of the National Academy of Sciences of the United States of America. 2013;110(23):E2098–105. doi:10.1073/pnas.1304382110.

12. Sánchez C, Bueno-Orovio A, Wettwer E, Loose S, Simon J, Ravens U, et al. Inter-subject variability in human atrial action potential in sinus rhythm versus chronic atrial fibrillation. PLoS ONE. 2014;9(8):e105897. doi:10.1371/journal.pone.0105897.

13. Muszkiewicz A, Britton OJ, Gemmell P, Passini E, Carlos S, Zhou X, et al. Variability in cardiac electrophysiology : Using experimentally- calibrated populations of models to move beyond the single virtual physiological human paradigm. Progress in Biophysics and Molecular Biology. 2015;120(2016):115–127. doi:10.1016/j.pbiomolbio.2015.12.002.

14. Clarke R, Ressom HW, Wang A, Xuan J, Liu MC. The properties of high-dimensional data spaces : implications for exploring gene and protein expression data. Nature Reviews Cancer. 2008;8(january):37–49. doi:10.1038/nrc2294.

15. Pathmanathan P, Cordeiro JM, Gray RA. Comprehensive Uncertainty Quantification and Sensitivity Analysis for Cardiac Action Potential Models. Frontiers in Physiology. 2019;10(June):1–20. doi:10.3389/fphys.2019.00721.

16. Mirams GR, Pathmanathan P, Gray Ra, Challenor P, Clayton RH. White paper: Uncertainty and variability in computational and mathematical models of cardiac physiology. The Journal of physiology. 2016;epub aheea:1–33. doi:10.1113/JP271671.

17. Eck VG, Donders WP, Sturdy J. Advances in 0D and 1D models for circulation. A guide to uncertainty quantification and sensitivity analysis for cardiovascular applications. International Journal for Numerical Methods in Biomedical Engineering. 2016;32(8):e02755. doi:10.1002/cnm.

18. Chang ETY, Strong M, Clayton RH. Bayesian Sensitivity Analysis of a Cardiac Cell Model Using a Gaussian Process Emulator. PLoS ONE. 2015;10(6):e0130252. doi:10.1371/journal.pone.0130252.

19. Johnstone RH, Chang ETY, Bardenet R, de Boer TP, Gavaghan DJ, Pathmanathan P, et al. Uncertainty and variability in models of the cardiac action potential: Can we build trustworthy models? Journal of Molecular and Cellular Cardiology. 2015;96:49–62. doi:10.1016/j.yjmcc.2015.11.018.

bioRxiv preprint doi: https://doi.org/10.1101/818047; this version posted October 24, 2019. The copyright holder for this preprint (which was not certified by peer review) is the author/funder, who has granted bioRxiv a license to display the preprint in perpetuity. It is made available under aCC-BY 4.0 International license.

20. Courtemanche M, Ramirez RJ, Nattel S. Ionic mechanisms underlying human atrial action potential properties: insights from a mathematical model. The American Journal of Physiology. 1998;275:H301–H321.

21. Nygren A, Fiset C, Firek L, Clark JW, Lindblad DS, Clark RB, et al. Mathematical Model of an Adult Human Atrial Cell The Role of K Currents in Repolarization. Circulation Research. 1998;82:63–81. doi:10.1161/01.RES.82.1.63.

22. Maleckar MM, Greenstein JL, Giles WR, Trayanova Na. K+ current changes account for the rate dependence of the action potential in the human atrial myocyte. American journal of physiology Heart and circulatory physiology. 2009;297(4):H1398–H1410. doi:10.1152/ajpheart.00411.2009.

23. Colman MA, Aslanidi OV, Kharche S, Boyett MR, Garratt CJ, Hancox JC, et al. Pro-arrhythmogenic Effects of Atrial Fibrillation Induced Electrical Remodelling-Insights from 3D Virtual Human Atria. Journal of Physiology (London). 2013;17(2013):4249–4272. doi:10.1113/jphysiol.2013.254987.

24. Krogh-Madsen T, Abbott GW, Christini DJ. Effects of electrical and structural remodeling on atrial fibrillation maintenance: a simulation study. PLoS computational biology. 2012;8(2):e1002390. doi:10.1371/journal.pcbi.1002390.

25. McDowell KS, Arevalo HJ, Maleckar MM, Trayanova NA. Susceptibility to arrhythmia in the infarcted heart depends on myofibroblast density. Biophysical Journal. 2011;101(6):1307–15. doi:10.1016/j.bpj.2011.08.009.

26. Tobón C, Ruiz-Villa CA, Heidenreich E, Romero L, Hornero F, Saiz J. A Three-Dimensional Human Atrial Model with Fiber Orientation. Electrograms and Arrhythmic Activation Patterns Relationship. PLoS ONE. 2013;8(2). doi:10.1371/journal.pone.0050883.

27. Oakley J, O'Hagan A. Bayesian inference for the uncertainty distribution of computer model outputs. Biometrika. 2002;89:769–784.

28. Oakley JE, O'Hagan A. Probabilistic sensitivity analysis of complex models: a Bayesian approach. Journal of the Royal Statistical Society: Series B (Statistical Methodology). 2004;66(3):751–769. doi:10.1111/j.1467-9868.2004.05304.x.

29. Kennedy MC, O'Hagan A. Bayesian calibration of computer models. Journal of the Royal Statistical Society: Series B (Statistical Methodology). 2001;63(3):425–464. doi:10.1111/1467-9868.00294.

30. Andrianakis I, Challenor PG. The effect of the nugget on Gaussian process emulators of computer models. Computational Statistics and Data Analysis. 2012;56(12):4215–4228. doi:10.1016/j.csda.2012.04.020.

31. Saltelli A, Aleksankina K, Becker W, Fennell P, Ferretti F, Holst N, et al. Why so many published sensitivity analyses are false: A systematic review of sensitivity analysis practices. Environmental Modelling and Software. 2019;114(January):29–39. doi:10.1016/j.envsoft.2019.01.012.

32. Sobie EA. Parameter sensitivity analysis in electrophysiological models using multivariable regression. Biophysical Journal. 2009;96(4):1264–74. doi:10.1016/j.bpj.2008.10.056.

33. Sarkar AX, Sobie Ea. Regression analysis for constraining free parameters in electrophysiological models of cardiac cells. PLoS Computational Biology. 2010;6(9):e1000914. doi:10.1371/journal.pcbi.1000914.

bioRxiv preprint doi: https://doi.org/10.1101/818047; this version posted October 24, 2019. The copyright holder for this preprint (which was not certified by peer review) is the author/funder, who has granted bioRxiv a license to display the preprint in perpetuity. It is made available under aCC-BY 4.0 International license.

34. Saltelli A, Ratto M, Tarantola S, Campolongo F. Update 1 of: Sensitivity analysis for chemical models. Chemical reviews. 2012;112(5):PR1–21. doi:10.1021/cr200301u.

35. Varela M, Colman MA, Hancox JC, Aslanidi OV. Atrial Heterogeneity Generates Re-entrant Substrate during Atrial Fibrillation and Anti-arrhythmic Drug Action: Mechanistic Insights from Canine Atrial Models. PLoS Computational Biology. 2016;12(12):1–22. doi:10.1371/journal.pcbi.1005245.

36. Krogh-Madsen T, Christini DJ. Nonlinear dynamics in cardiology. Annual Review of Biomedical Engineering. 2012;14:179–203. doi:10.1146/annurev-bioeng-071811-150106.

37. Cherry EM, Hastings HM, Evans SJ. Dynamics of human atrial cell models: restitution, memory, and intracellular calcium dynamics in single cells. Progress in Biophysics and Molecular Biology. 2008;98:24–37.

38. Zhang H, Garratt CJ, Zhu J, Holden AV. Role of up-regulation of IK1 in action potential shortening associated with atrial fibrillation in humans. Cardiovascular Research. 2005;66:493–502. doi:10.1016/j.cardiores.2005.01.020.

39. Melis A, Clayton RH, Marzo A. Bayesian sensitivity analysis of a 1D vascular model with Gaussian process emulators. International Journal for Numerical Methods in Biomedical Engineering. 2017;doi:10.1002/cnm.2882.

40. McKay MD, Beckman RJ, Conover WJ. Comparison of three methods for selecting values of input variables in the analysis of output from a computer code. Technometrics. 1979;21(2):239–245. doi:10.2307/1271432.

41. Bingham D, Sitter RR, Tang B. Orthogonal and nearly orthogonal designs for computer experiments. Biometrika. 2009;96(1):51–65. doi:10.1093/biomet/asn057.

42. Coveney S, Clayton RH. Fitting two human atrial cell models to experimental data using Bayesian history matching. Progress in Biophysics and Molecular Biology. 2018;139:43–58. doi:10.1016/j.pbiomolbio.2018.08.001.

43. Johnston BM, Coveney S, Chang ETY, Johnston PR, Clayton RH. Quantifying the effect of uncertainty in input parameters in a simplified bidomain model of partial thickness ischaemia. Medical and Biological Engineering and Computing. 2018;56(5):761–780. doi:10.1007/s11517-017-1714-y.

44. Chang ETY, Coveney S, Clayton RH. Variance Based Sensitivity Analysis of IKr in a Model of the Human Atrial Action Potential Using Gaussian Process Emulators. Functional Imaging and Modelling of the Heart. 2017;10263:249–259. doi:10.1007/978-3-319-59448-4.

45. Beattie KA, Hill AP, Bardenet R, Cui Y, Vandenberg JI, Gavaghan DJ, et al. Sinusoidal voltage protocols for rapid characterisation of ion channel kinetics. Journal of Physiology. 2018;596(10):1813–1828. doi:10.1113/JP275733.

46. Ghosh S, Gavaghan DJ, Mirams GR. Gaussian process emulation for discontinuous response surfaces with applications for cardiac electrophysiology models. arXiv preprint. 2018; p. 1805.10020.

47. Conti S, Gosling JP, Oakley JE, O'Hagan a. Gaussian process emulation of dynamic computer codes. Biometrika. 2009;96(3):663–676. doi:10.1093/biomet/asp028.

bioRxiv preprint doi: https://doi.org/10.1101/818047; this version posted October 24, 2019. The copyright holder for this preprint (which was not certified by peer review) is the author/funder, who has granted bioRxiv a license to display the preprint in perpetuity. It is made available under aCC-BY 4.0 International license.

48. Conti S, O'Hagan A. Bayesian emulation of complex multi-output and dynamic computer models. Journal of Statistical Planning and Inference. 2010;140(3):640–651. doi:10.1016/j.jspi.2009.08.006.

49. Lawson BA, Burrage K, Burrage P, Drovandi CC, Bueno-Orovio A. Slow recovery of excitability increases ventricular fibrillation risk as identified by emulation. Frontiers in Physiology. 2018;9(AUG):1–19. doi:10.3389/fphys.2018.01114.

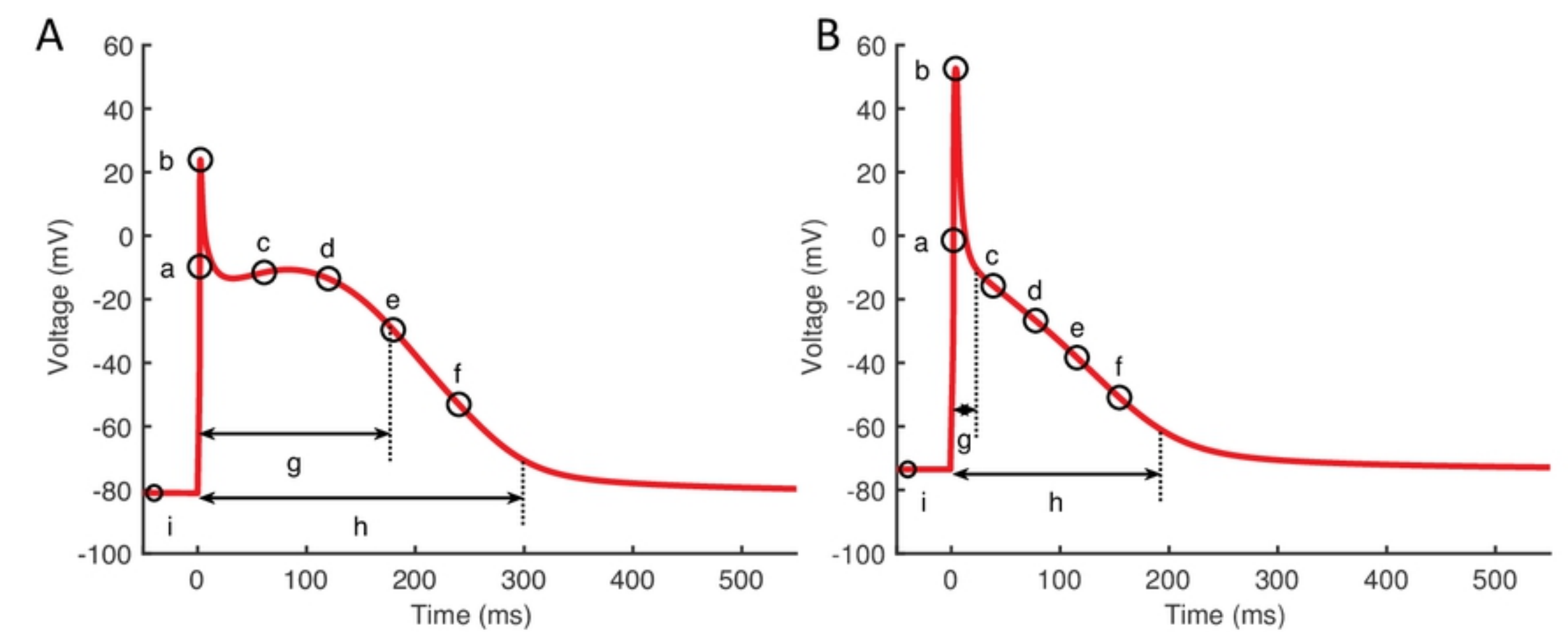
A
B
Voltage (mV)
Time (ms)
a
b
c
d
e
f
g
h
i
60
40
20
0
-20
-40
-60
-80
-100
0
100
200
300
400
500

Figure 1

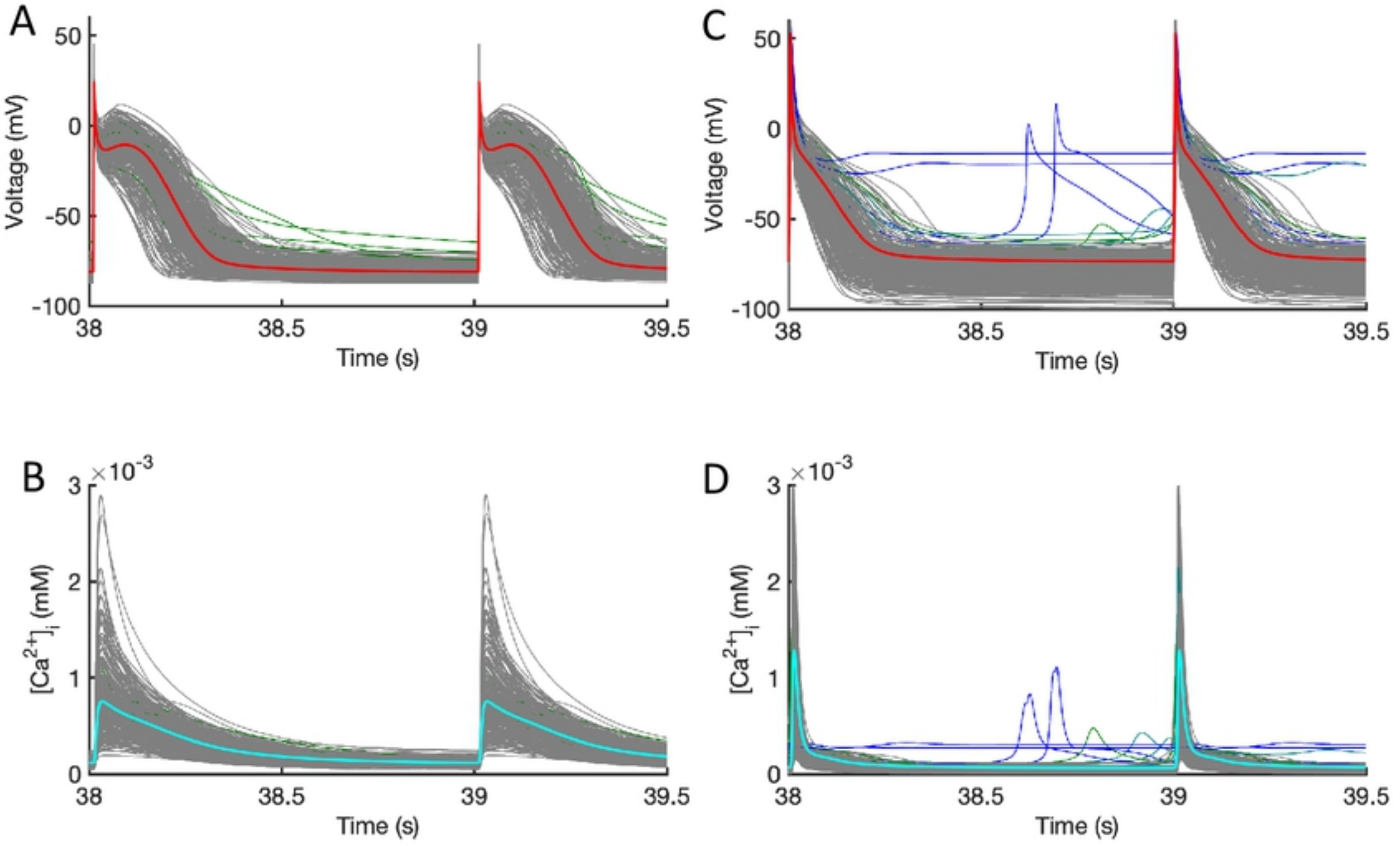
A
Voltage (mV)
50
0
-50
-100
38
38.5
39
39.5
Time (s)
C
Voltage (mV)
50
0
-50
-100
38
38.5
39
39.5
Time (s)
B
×10^-3
3
2
1
0
[Ca2+]i (mM)
38
38.5
39
39.5
Time (s)
D
×10^-3
3
2
1
0
[Ca2+]i (mM)
38
38.5
39
39.5
Time (s)

Figure 2

bioRxiv preprint doi: https://doi.org/10.1101/818047; this version posted October 24, 2019. The copyright holder for this preprint (which was not certified by peer review) is the author/funder, who has granted bioRxiv a license to display the preprint in perpetuity. It is made available under aCC-BY 4.0 International license.

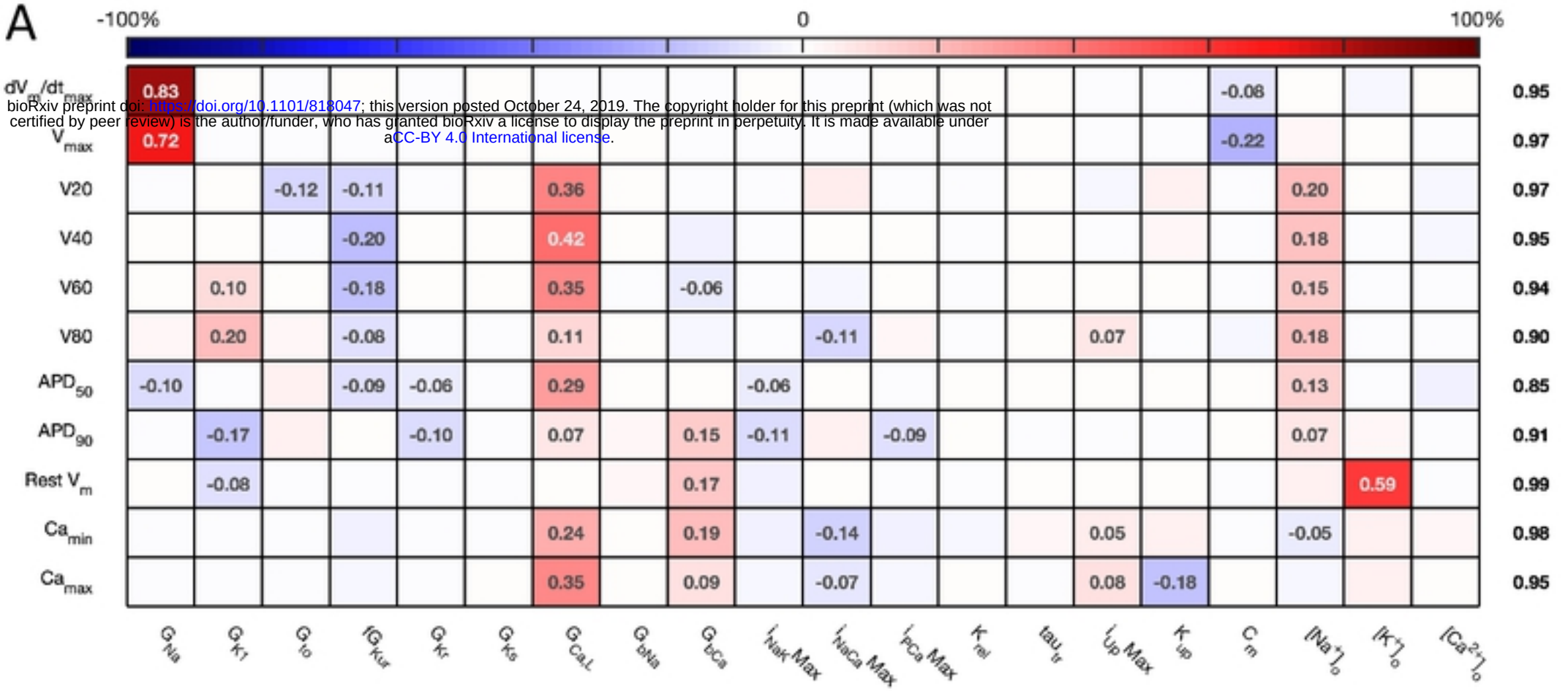

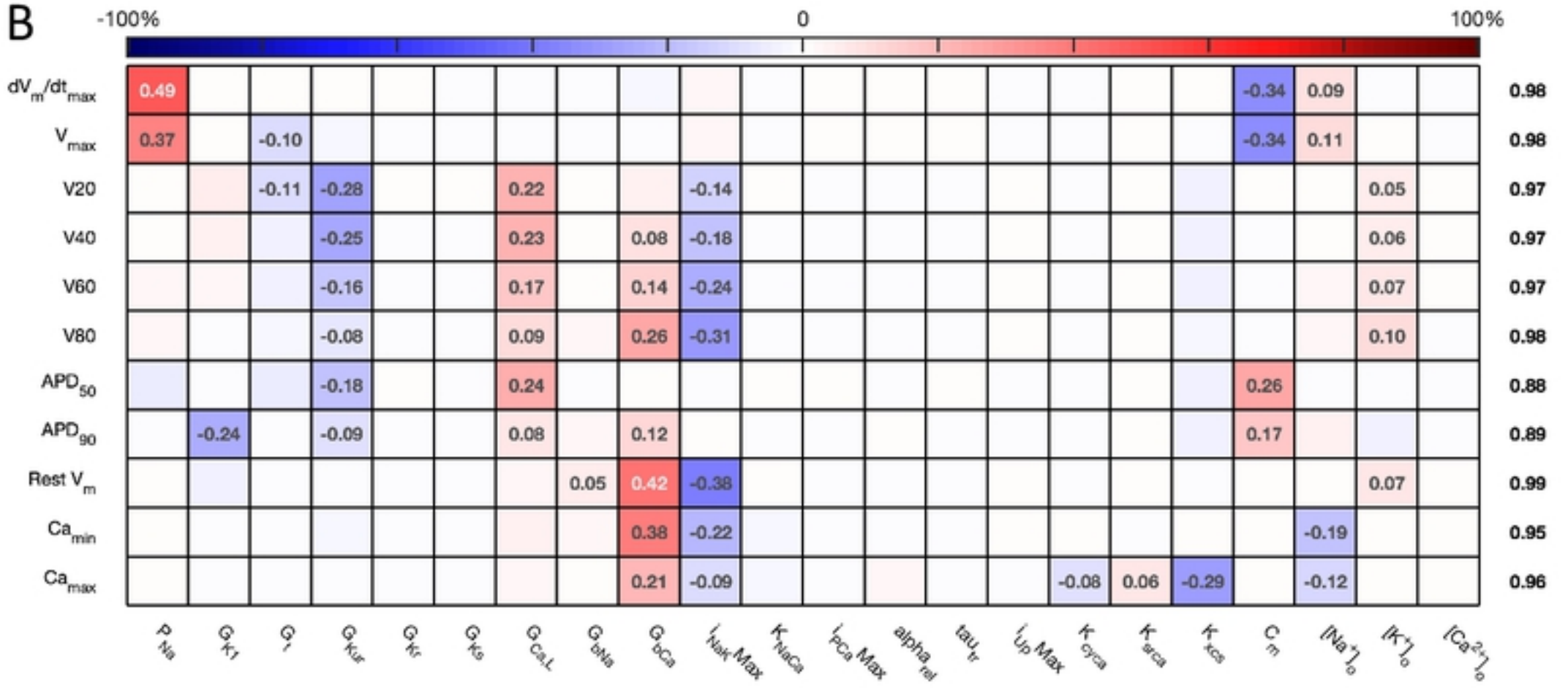

Figure 3

bioRxiv preprint doi: https://doi.org/10.1101/818047; this version posted October 24, 2019. The copyright holder for this preprint (which was not certified by peer review) is the author/funder, who has granted bioRxiv a license to display the preprint in perpetuity. It is made available under aCC-BY 4.0 International license.

A

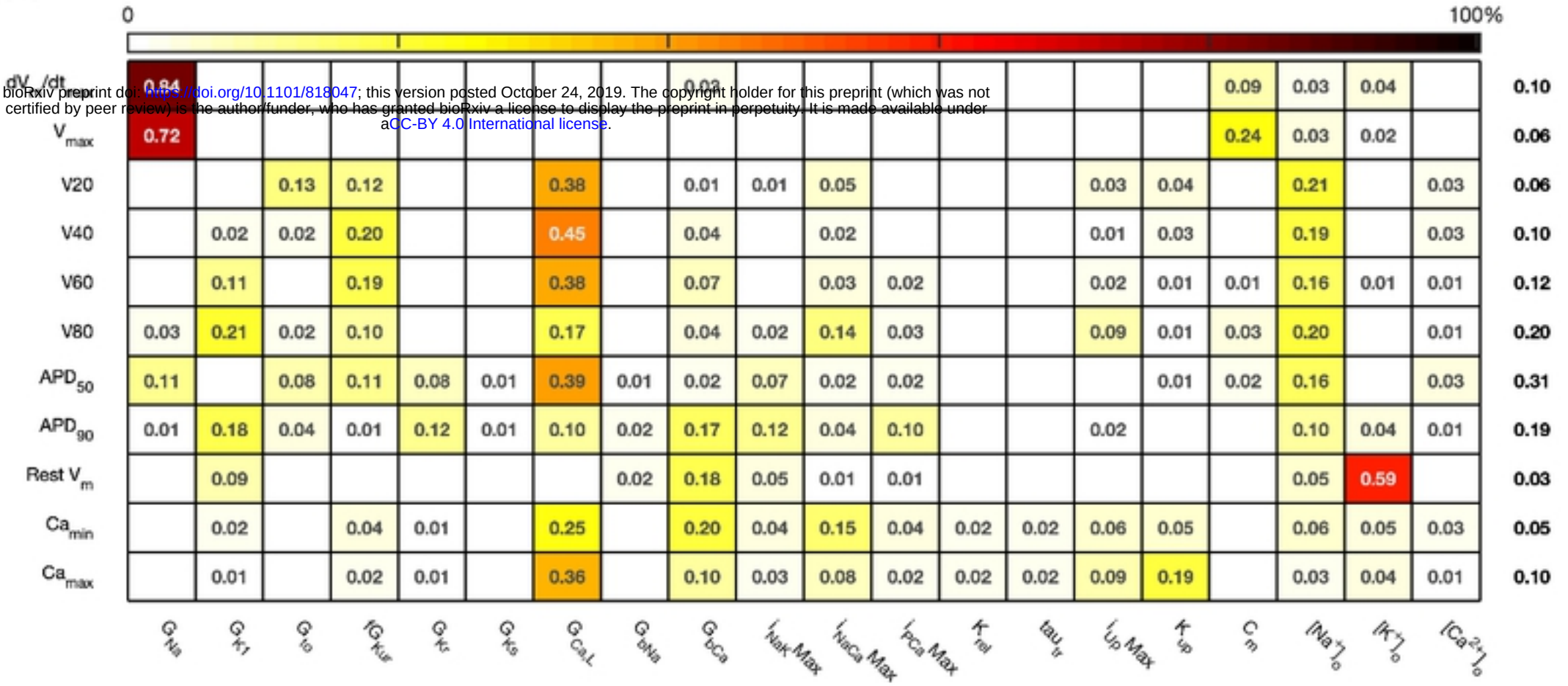

B

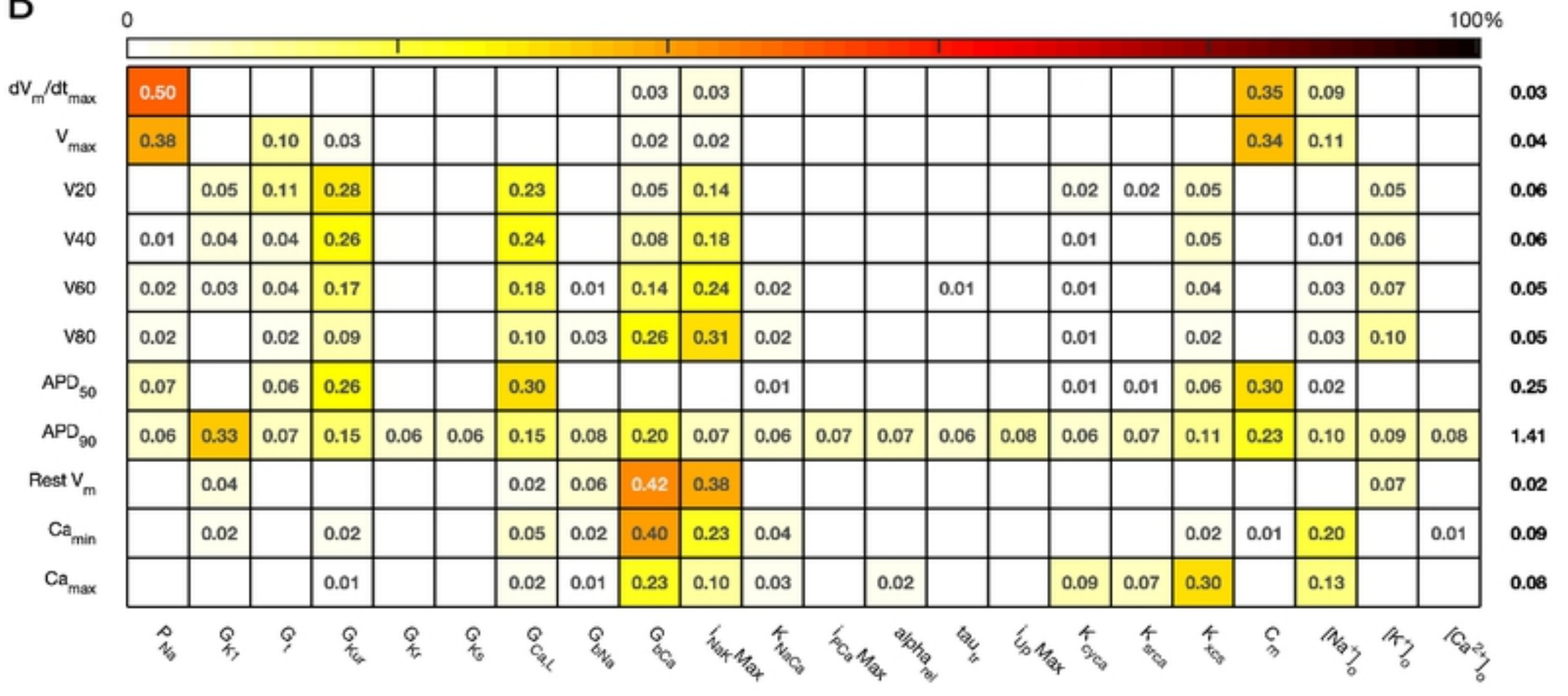

Figure 4

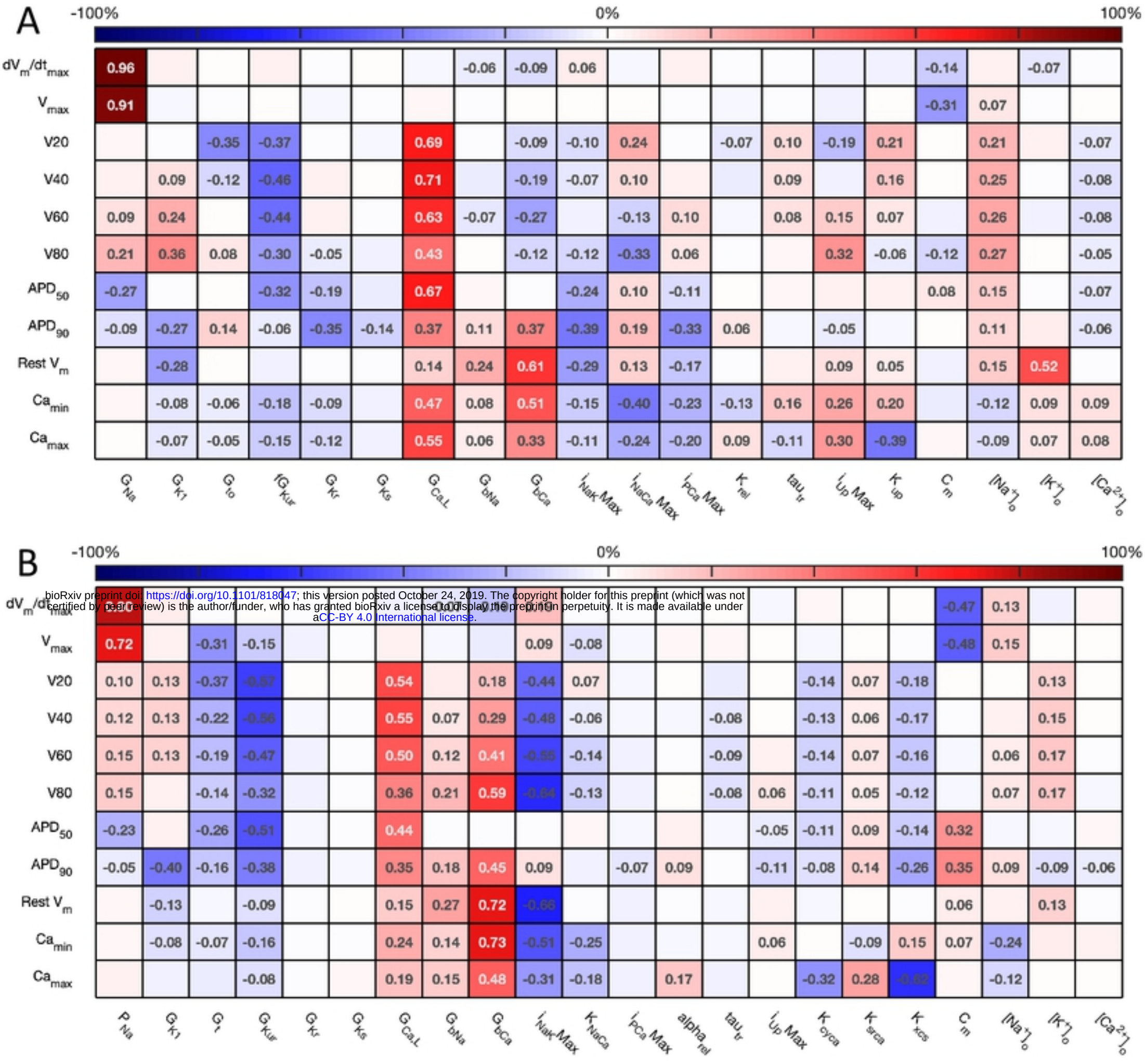

bioRxiv preprint doi: https://doi.org/10.1101/818047; this version posted October 24, 2019. The copyright holder for this preprint (which was not certified by peer review) is the author/funder, who has granted bioRxiv a license to display the preprint in perpetuity. It is made available under aCC-BY 4.0 International license.

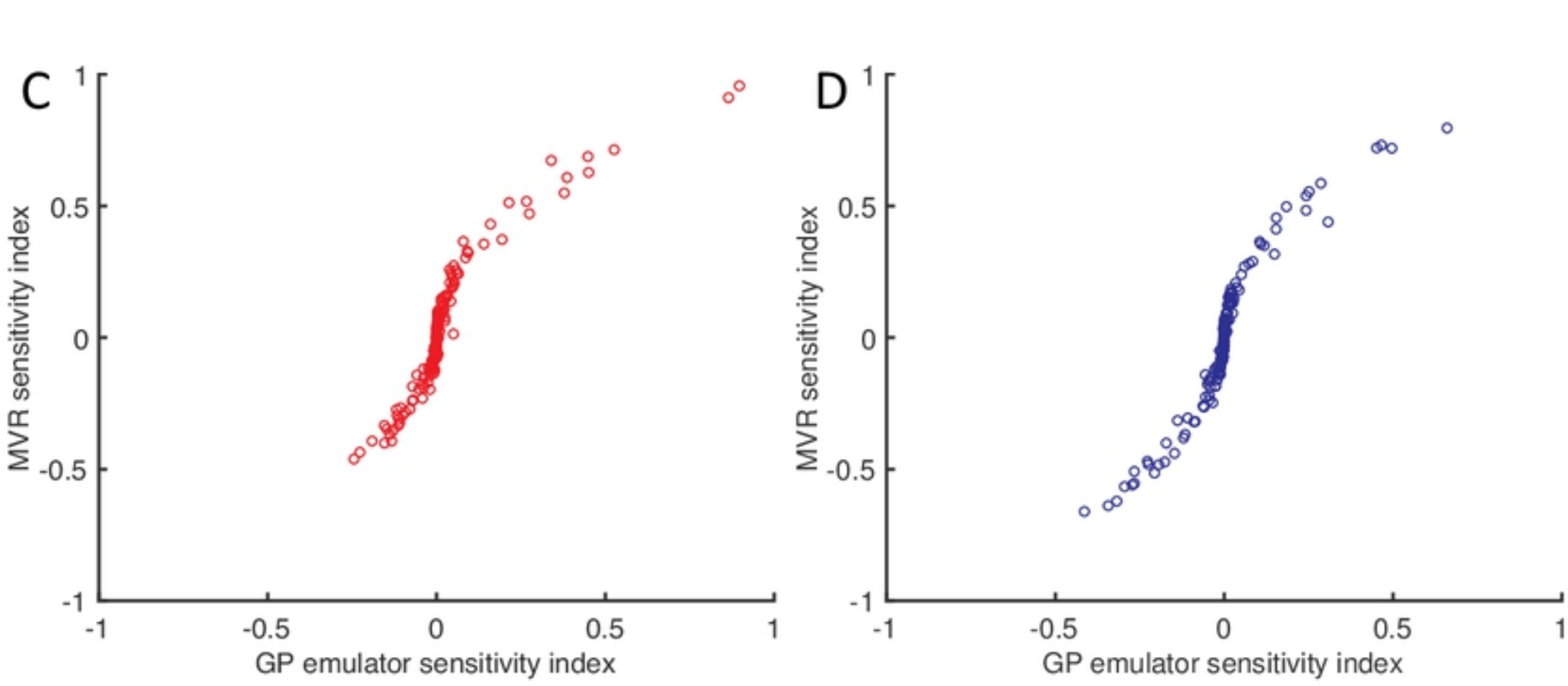

Figure 5

bioRxiv preprint doi: https://doi.org/10.1101/818047; this version posted October 24, 2019. The copyright holder for this preprint (which was not certified by peer review) is the author/funder, who has granted bioRxiv a license to display the preprint in perpetuity. It is made available under aCC-BY 4.0 International license.

A

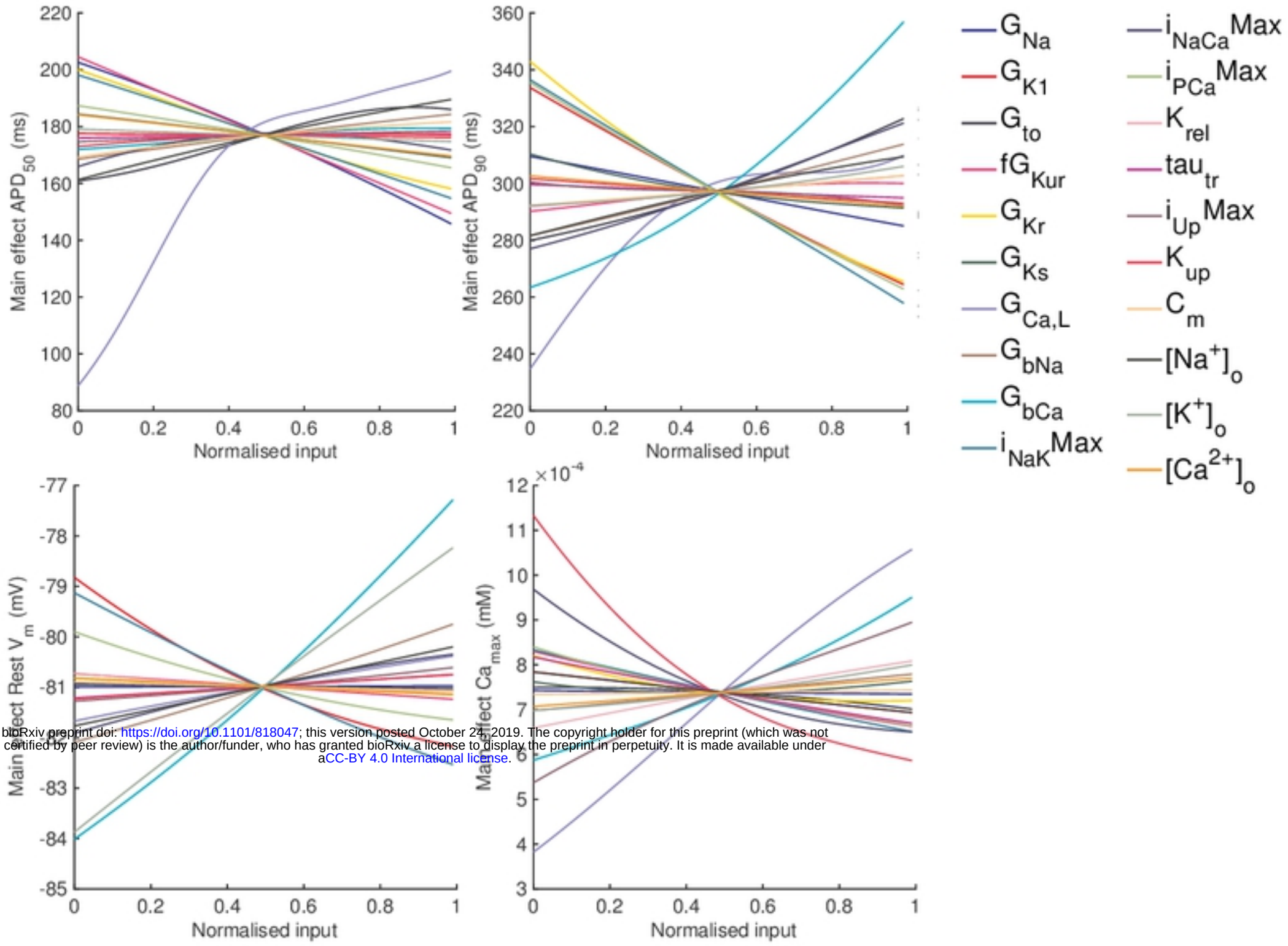

B

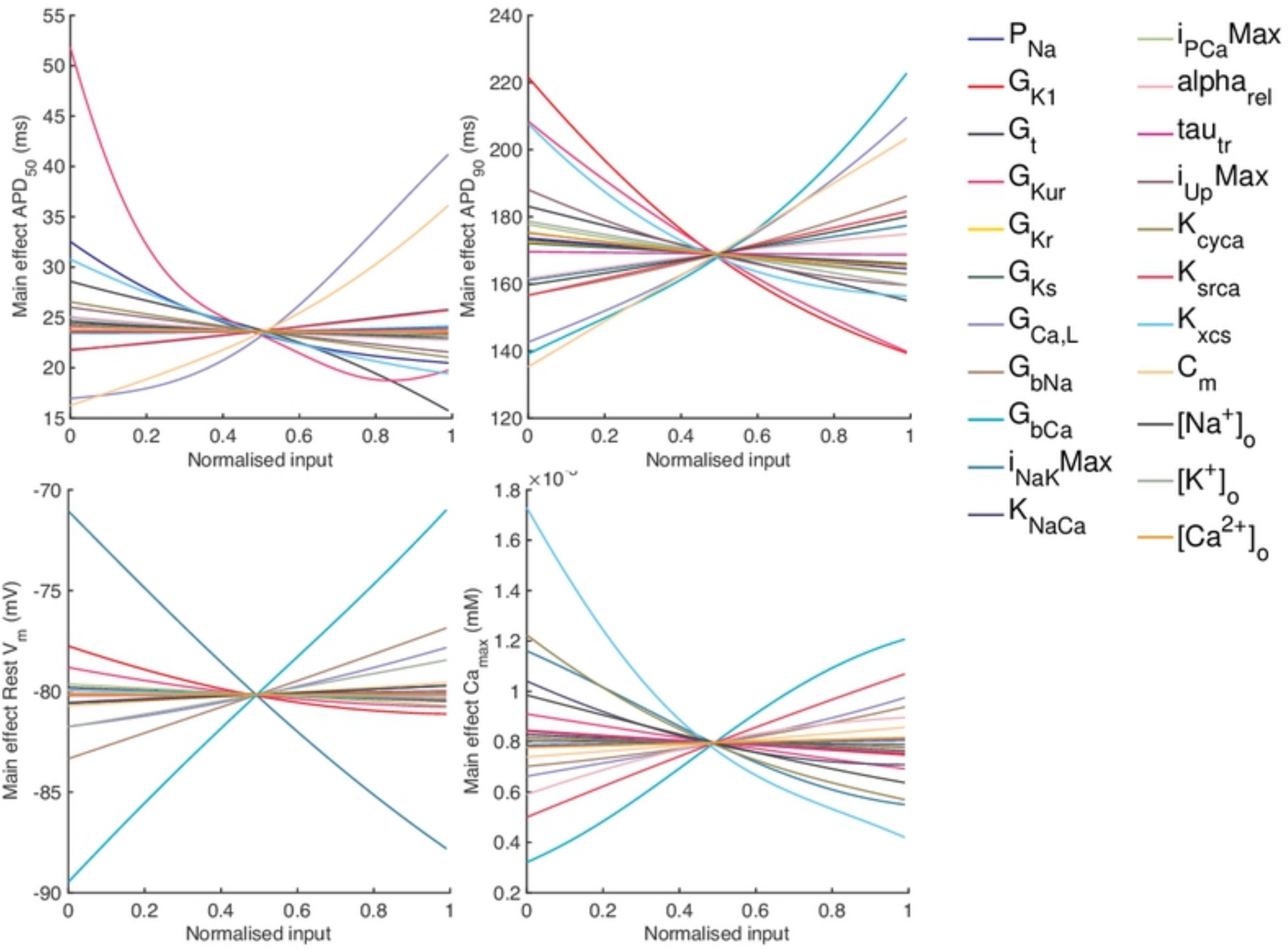

Figure 6

bioRxiv preprint doi: https://doi.org/10.1101/818047; this version posted October 24, 2019. The copyright holder for this preprint (which was not certified by peer review) is the author/funder, who has granted bioRxiv a license to display the preprint in perpetuity. It is made available under aCC-BY 4.0 International license.

A

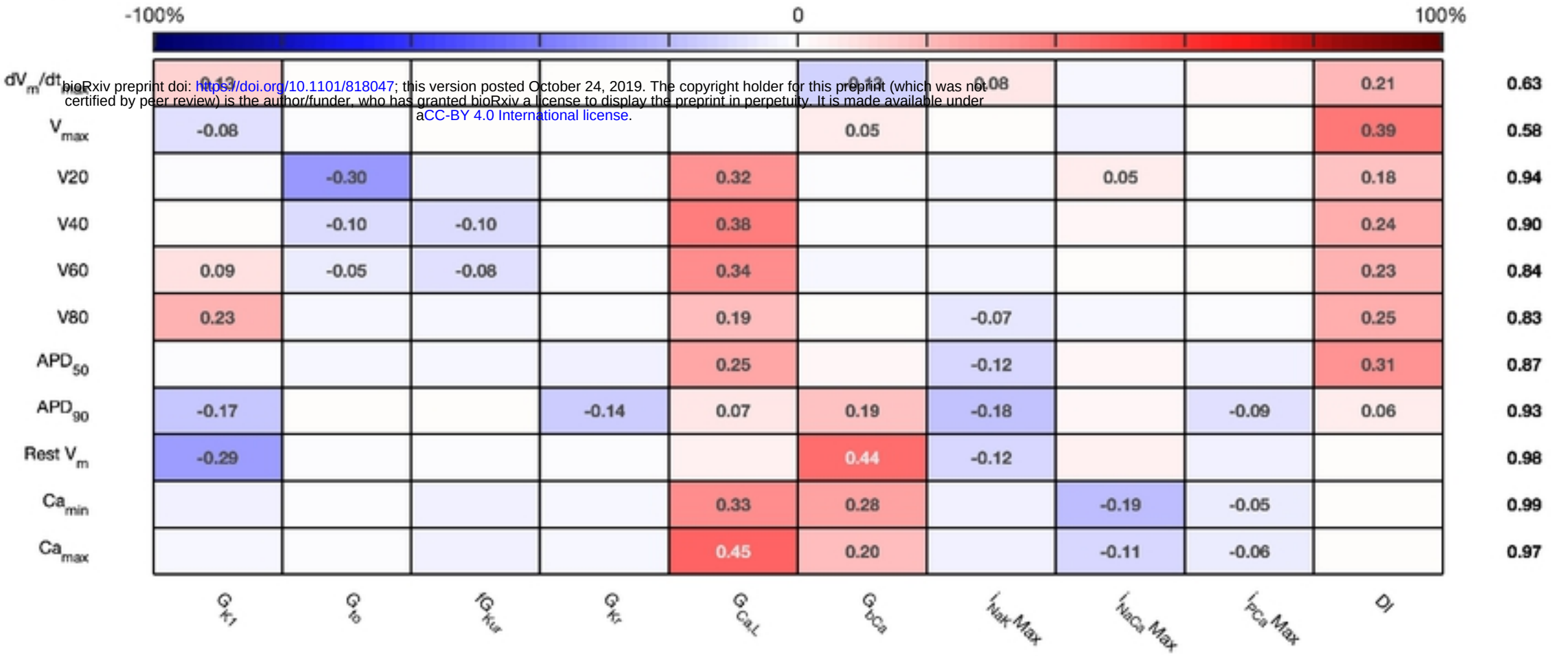

B

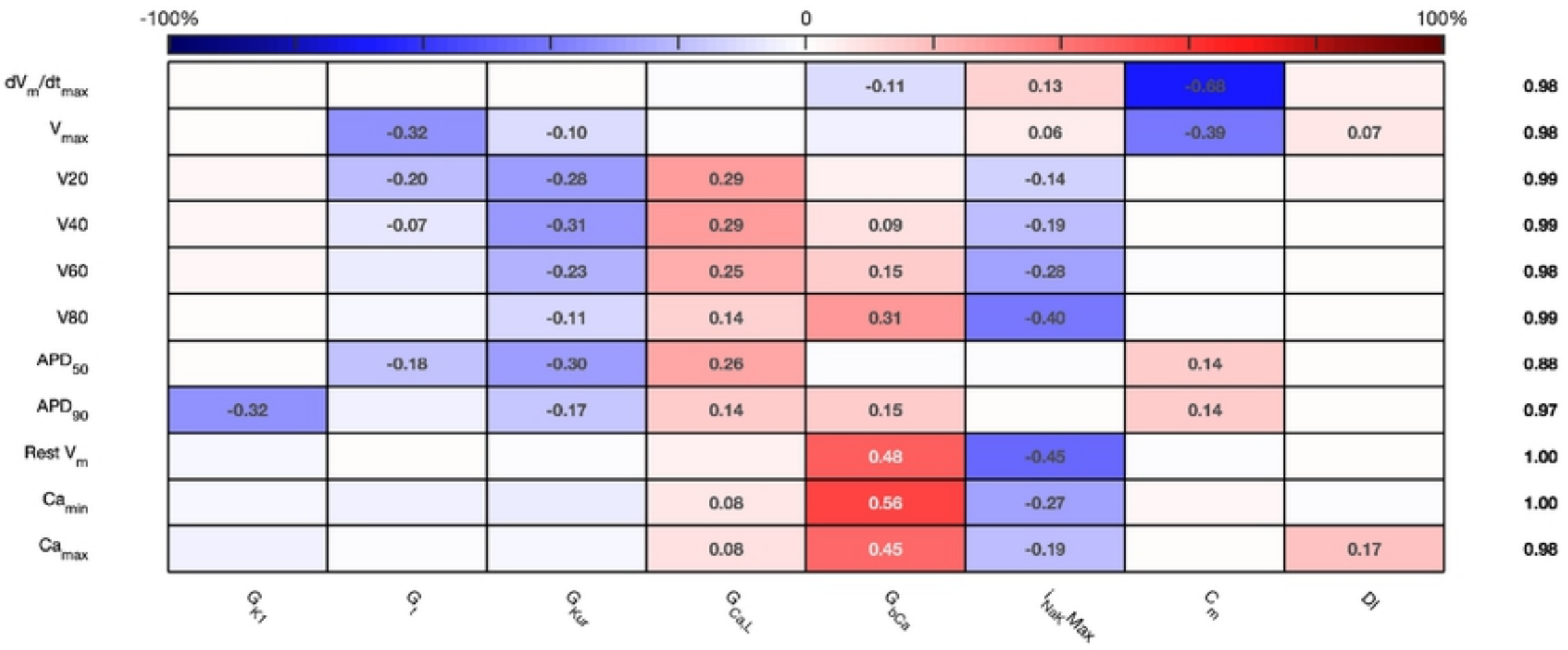

Figure 7

bioRxiv preprint doi: https://doi.org/10.1101/818047; this version posted October 24, 2019. The copyright holder for this preprint (which was not certified by peer review) is the author/funder, who has granted bioRxiv a license to display the preprint in perpetuity. It is made available under aCC-BY 4.0 International license.

A

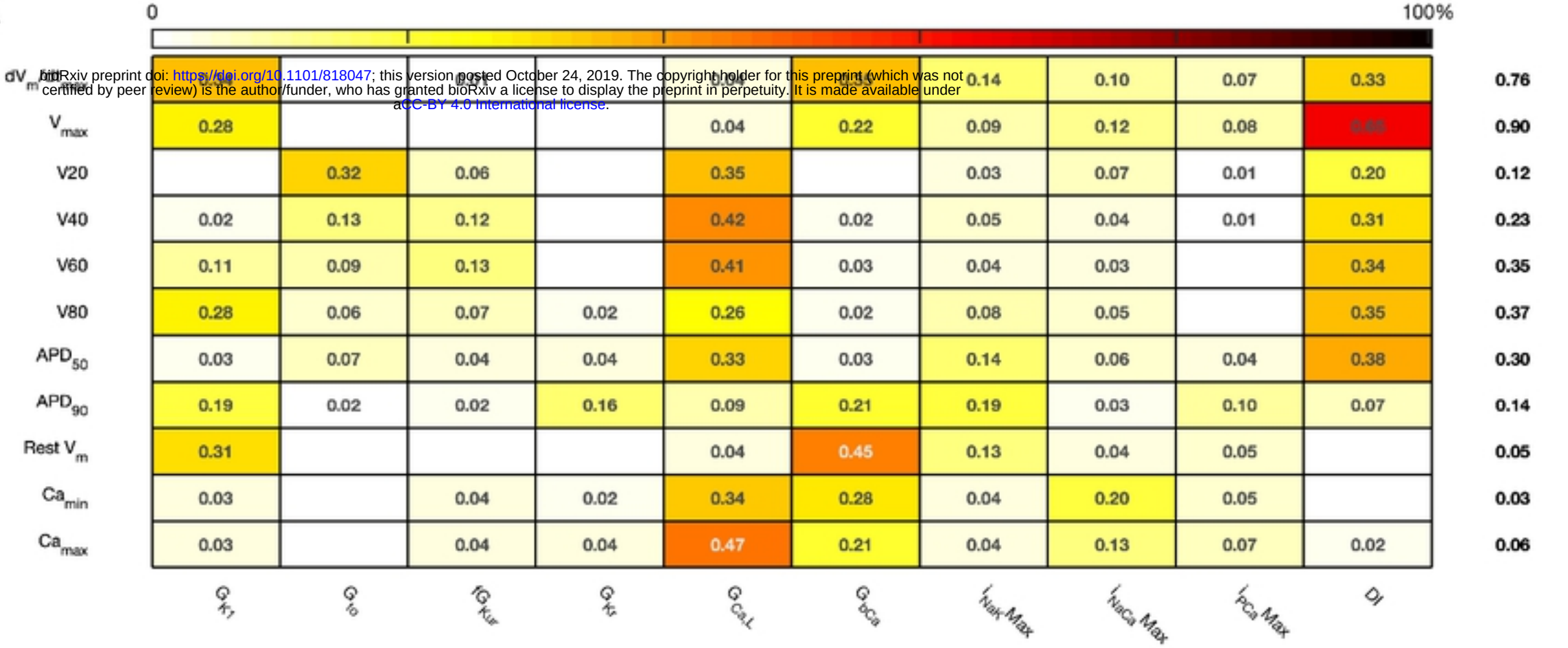

B

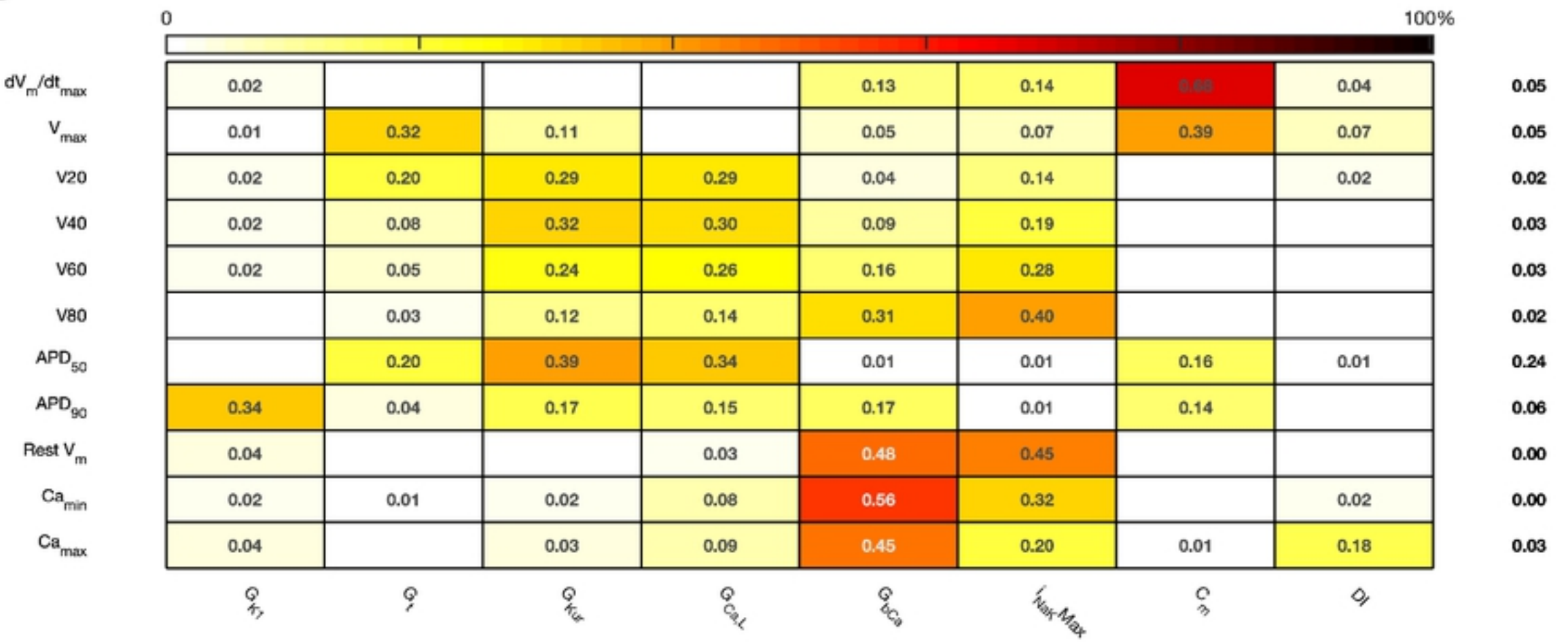

Figure 8

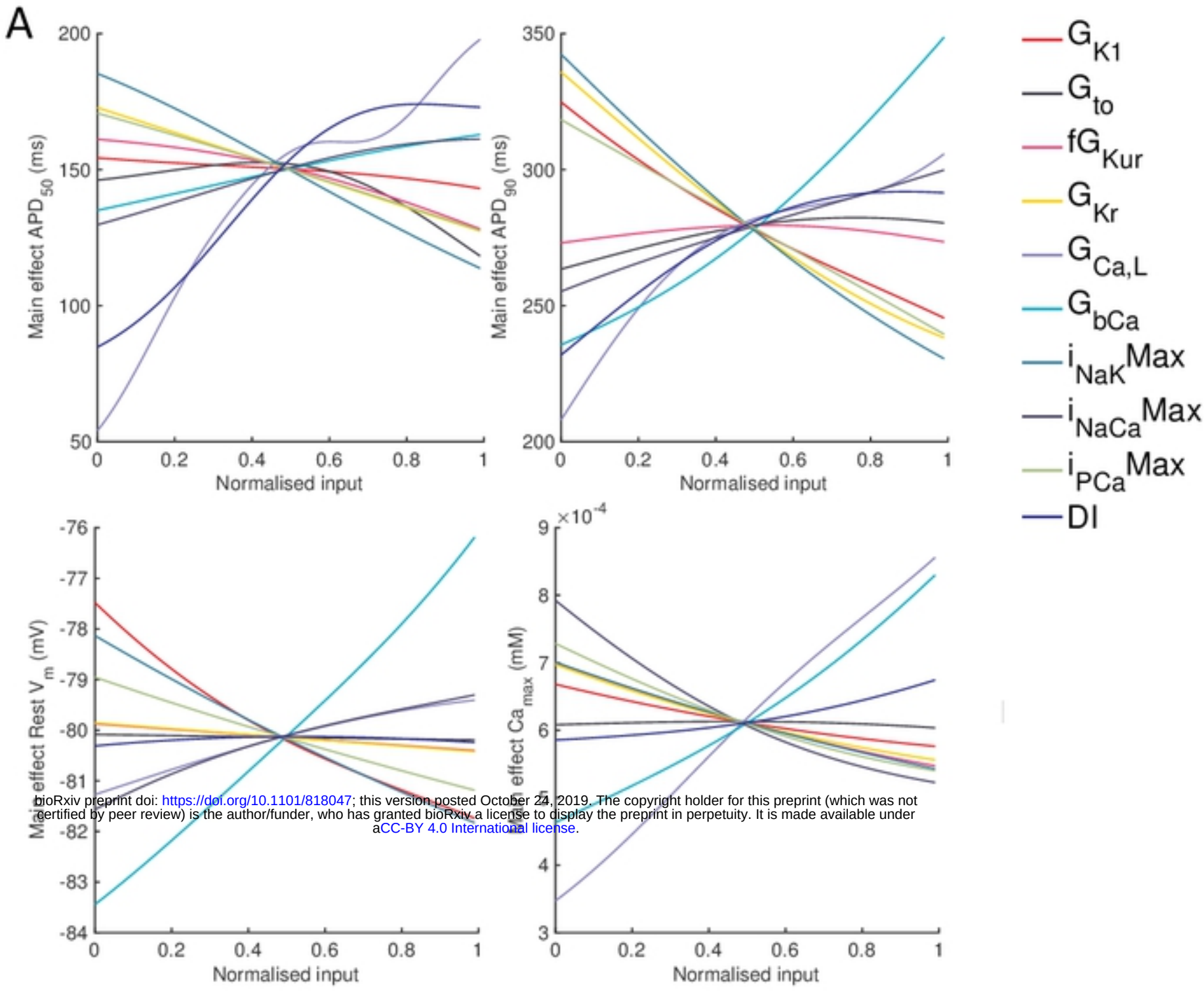

bioRxiv preprint doi: https://doi.org/10.1101/818047; this version posted October 24, 2019. The copyright holder for this preprint (which was not certified by peer review) is the author/funder, who has granted bioRxiv a license to display the preprint in perpetuity. It is made available under aCC-BY 4.0 International license.

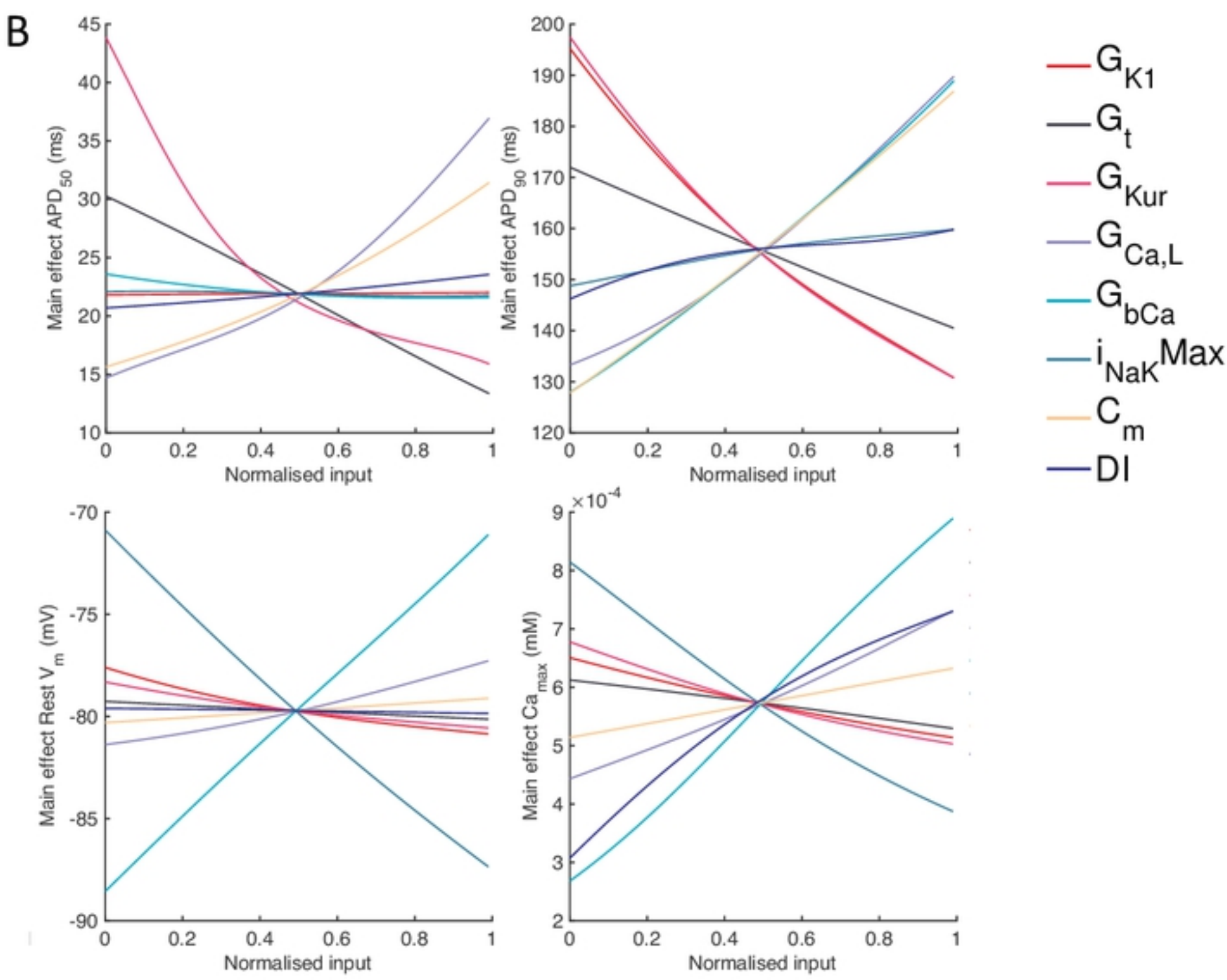

Figure 9

bioRxiv preprint doi: https://doi.org/10.1101/818047; this version posted October 24, 2019. The copyright holder for this preprint (which was not certified by peer review) is the author/funder, who has granted bioRxiv a license to display the preprint in perpetuity. It is made available under aCC-BY 4.0 International license.

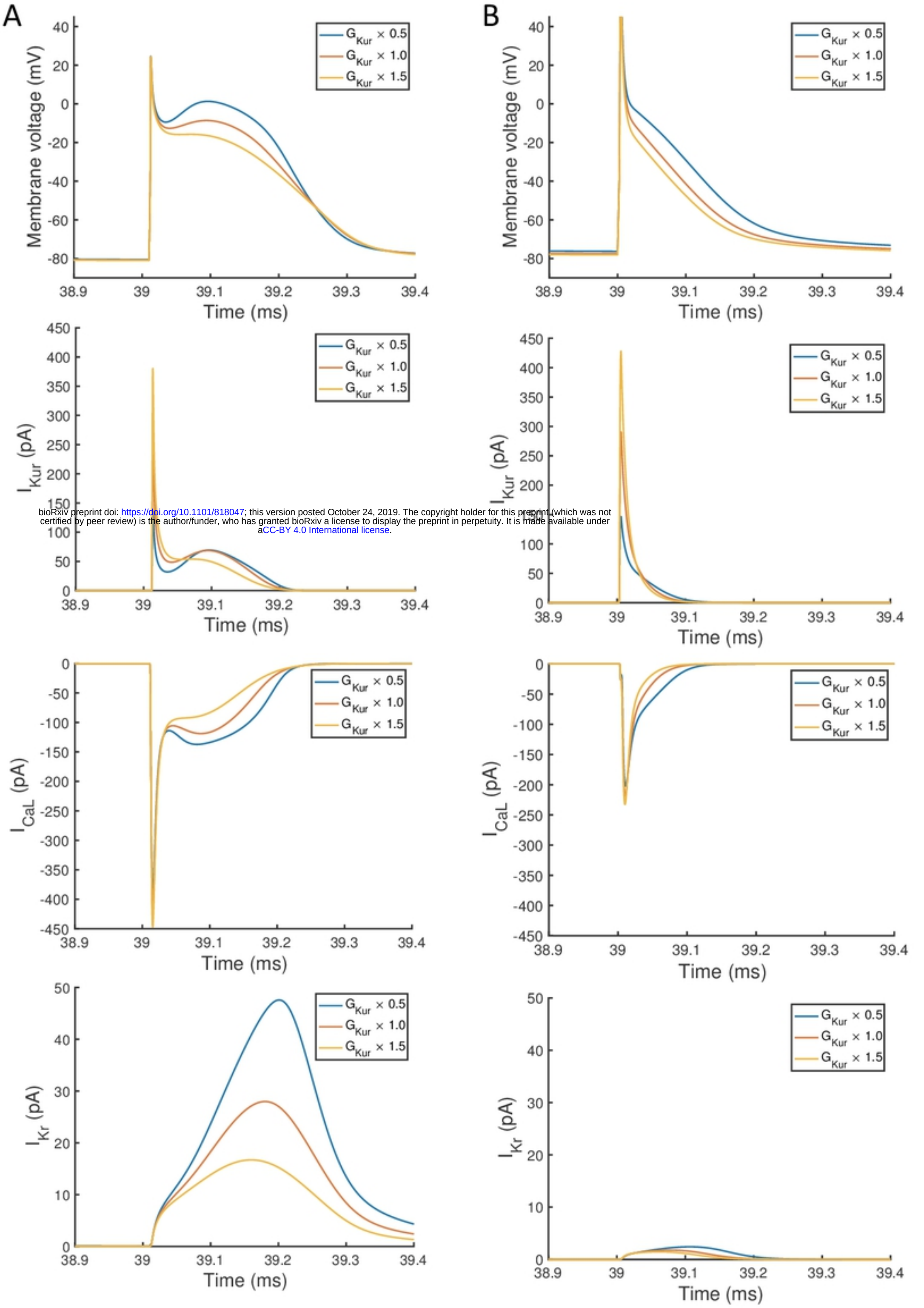

Figure 10

bioRxiv preprint doi: https://doi.org/10.1101/818047; this version posted October 24, 2019. The copyright holder for this preprint (which was not certified by peer review) is the author/funder, who has granted bioRxiv a license to display the preprint in perpetuity. It is made available under aCC-BY 4.0 International license.

Figure 11

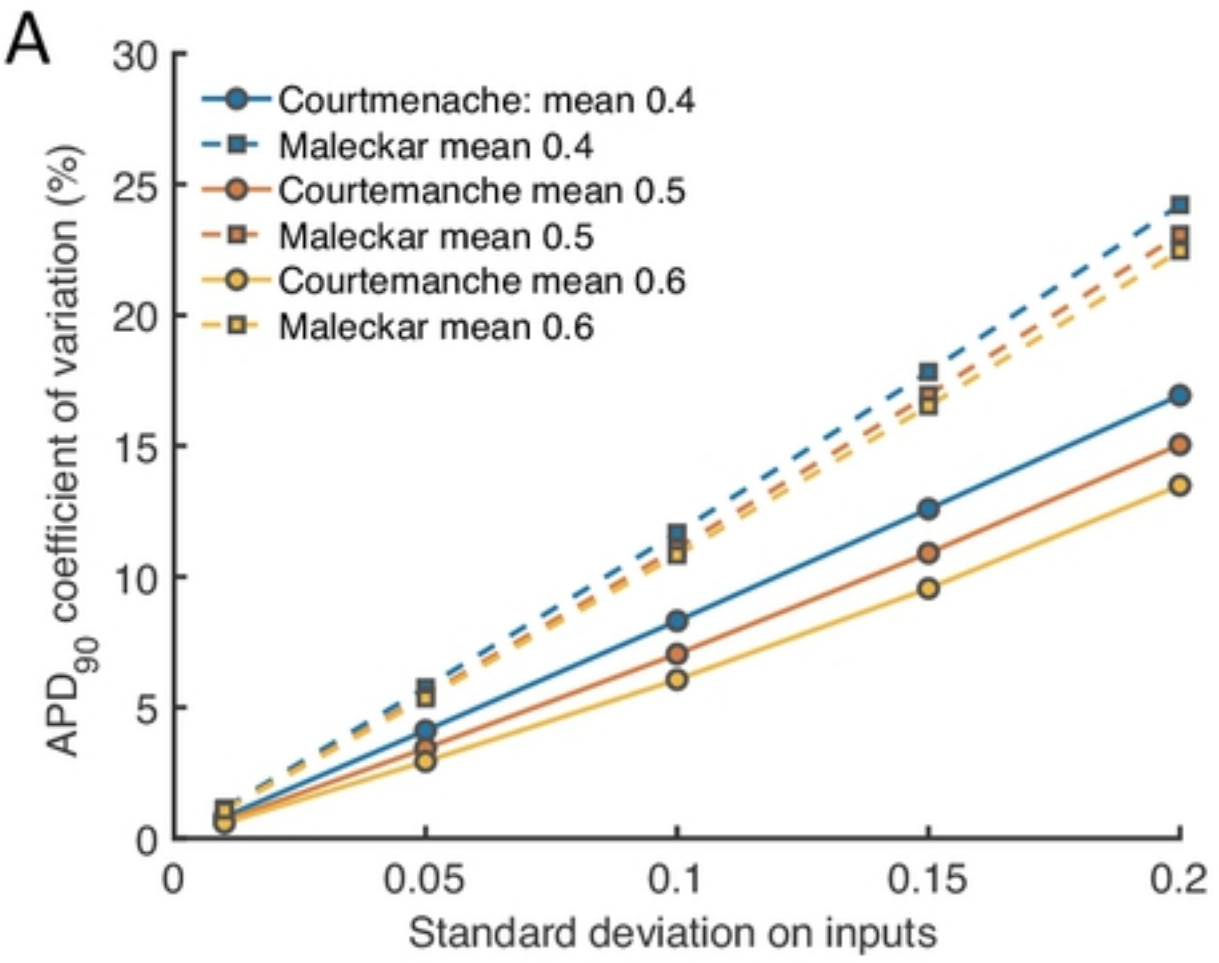

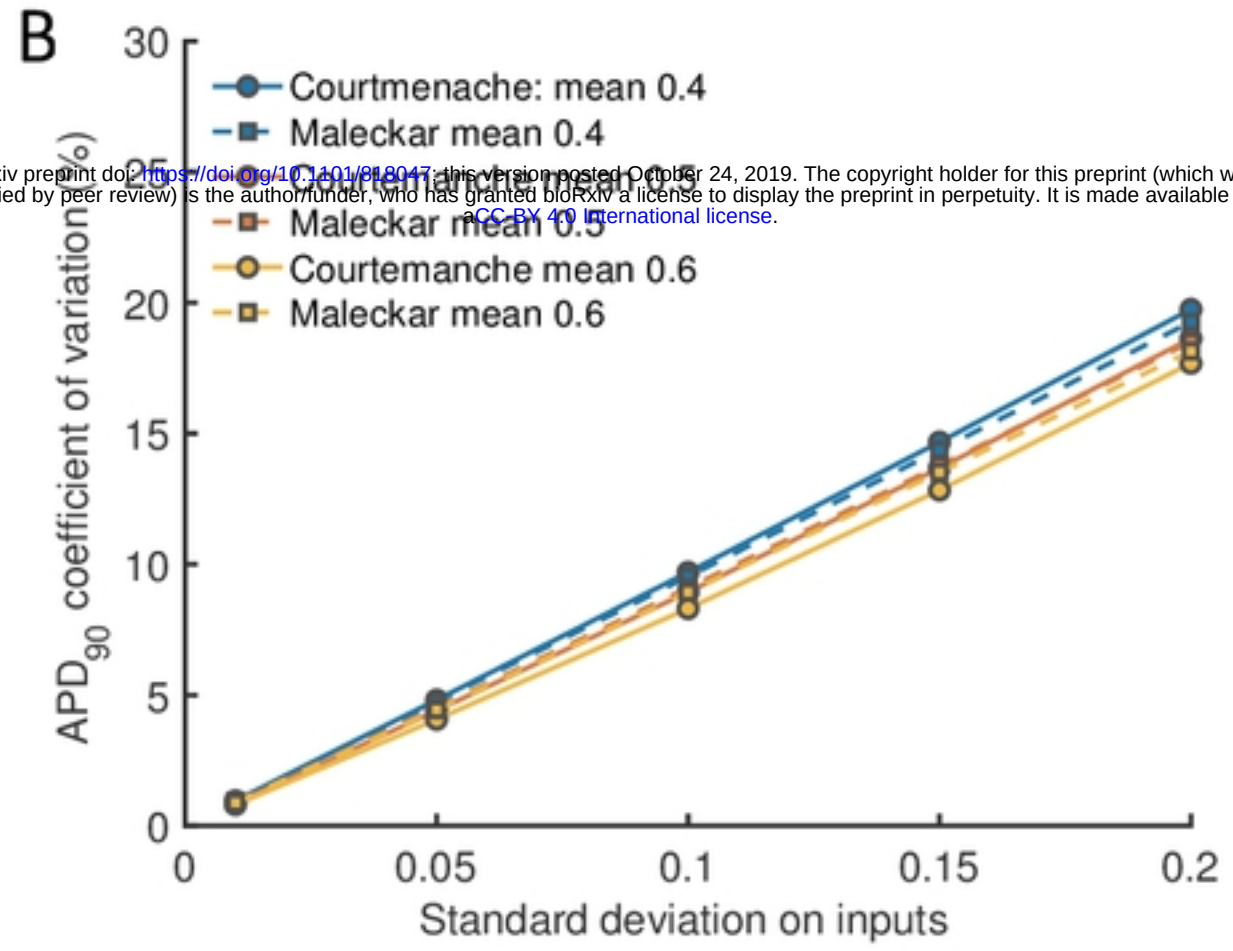

bioRxiv preprint doi: https://doi.org/10.1101/818047; this version posted October 24, 2019. The copyright holder for this preprint (which was not certified by peer review) is the author/funder, who has granted bioRxiv a license to display the preprint in perpetuity. It is made available under aCC-BY 4.0 International license.

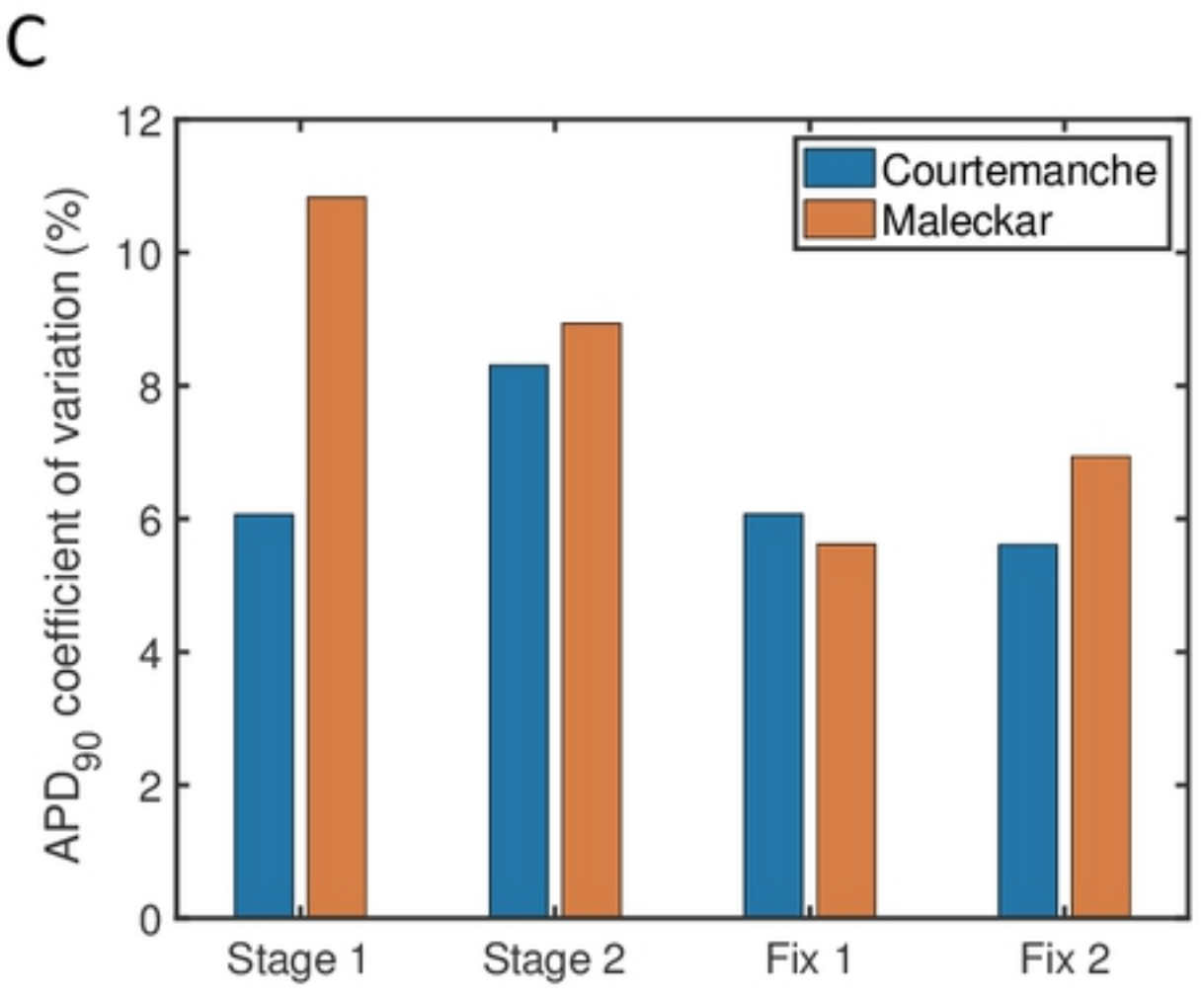

Figure 12